Investigation of Water/Oxide Interfaces by Molecular Dynamics Simulations

Ruiyu Wang[1,2], Michael L. Klein[1,2,3], Vincenzo Carnevale[3,4] and Eric Borguet[1,2*]*

[1]Department of Chemistry, Temple University, Philadelphia, Pennsylvania 19122, United States

[2] Center for Complex Materials from First Principles (CCM), Temple University, 1925 North 12th Street, Philadelphia, Pennsylvania 19122, United States

[3]Institute for Computational Molecular Science, Temple University, Philadelphia, Pennsylvania 19122, United States

[4]Department of Biology, Temple University, Philadelphia, Pennsylvania 19122, United States

ABSTRACT

Water/oxide interfaces are ubiquitous on earth and show significant influence on many chemical processes. For example, understanding water and solute adsorption as well as catalytic water splitting can help build better fuel cells and solar cells to overcome our

looming energy crisis; the interaction between biomolecules and water/oxide interfaces is one hypothesis to explain the origin of life. However, knowledge in this area is still limited due to the difficulty of studying water/solid interfaces. As a result, research using increasingly sophisticated experimental techniques and computational simulations has been carried out in recent years. Although it is difficult for experimental techniques to provide detailed microscopic structural information, molecular dynamics simulations have satisfactory performance. In this review, we discuss classical and ab initio molecular dynamics simulations of water/oxide interfaces. Generally, we are interested in the following questions: How do solid surfaces perturb interfacial water structure? How do interfacial water molecules and adsorbed solutes affect solid surfaces and how do interfacial environments affect solvent and solute behavior? Finally, we discuss progress in the application of neural network potential based molecular dynamics simulations, which we believe to be a promising future for MD simulations because such techniques can potentially achieve ab initio level accuracy with classical level cost.

Introduction

As one of the most ubiquitous substances on earth, water plays important role in innumerable chemical processes. One particular system, the water/solid interface, has close relationships to geochemistry, electrochemistry, environment chemistry and catalysis, and this attracts significant research interest.[1-4] For example, amino acid condensations, an important step of the origin of life, are more favored at mineral surfaces than in bulk water;[5, 6] water/platinum interfaces are widely used as electrodes for electrochemistry applications;[7] hydrogen fuel, believed to be one of the solutions to energy crisis, can be produced via water oxidation or hydrogen evolution reactions catalyzed by manganese oxide or MoS_2,[8, 9] and investigating these water/material interfaces can reveal the catalytic mechanisms and lead to the optimization of material design. In recent years, thousands of research papers have been published, but many fundamental questions, such as how far away from the solid surface is the solvent affected, how adsorbed solutes perturb interfacial water and the solid surfaces, and how chemical reactions at interfaces are different from those in the bulk, are still unknown or controversial.

A number of electrical double layer theory (EDL) models have been developed for describing the structure of charged solid/water interfaces.[10] In these models, the solid surface is treated as a homogenous infinite flat charged panel without any microscopic description of the chemical structure, and water is implicitly present as a continuum dielectric. The first primitive EDL model was proposed about 100 years ago by Helmholtz and is still the starting point of the more sophisticated understanding that has evolved since.[11] In this model, the solid surface is thought to be homogenously charged and the counter ions in water are attracted to the solid surface to offset its electric field, leading to a complete drop of the potential, so that beyond this compact counter ion layer the potential is zero.[11] Later, Gouy and Chapman suggested that the counter ions are adsorbed but not tightly bound to the surface.[12] By applying the Debye-Hückel theory and solving the Poisson-Boltzmann equation, they found that the electric potential shows an exponential decay with increasing distance from the surface.[13, 14] Nowadays, the most widely used EDL model is the Gouy-Chapman-Stern model (Figure 1).[15] Stern combined the models of Helmholtz and Gouy-Chapman: some ions adsorbed to the surface as per the Helmholtz model, forming a compact layer (a.k.a. Stern layer), but not screen the entire electric field; beyond the Stern layer (a.k.a. diffuse layer), the electric potential decays exponentially as the Gouy-Chapman model predicts.[16, 17] However, those approximations are problematic since charges are not always uniformly distributed at solid surfaces but may be located on some specific sites, leading to ion specific adsorption that the EDL model is not able to deal with.[18] A more important drawback of EDL models is that they do not take the types of ions into consideration, as a result, the effect of the size and polarization of the ions is missing.

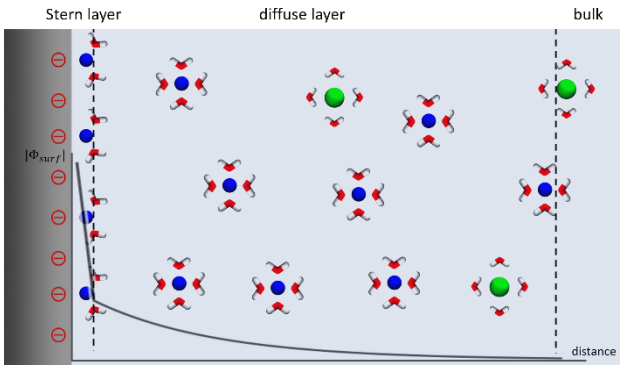

Figure 1. A snapshot of a surface following the Gouy-Chapman-Stern model. At the interface, cations are in excess because the mineral surface is negatively charged. Legend: blue, green balls represent positive, negative ions, respectively; red and white sticks represent the hydration shells of ions.

Researchers have developed various experimental techniques, such as X-ray reflectivity (XRR),[19] atomic force microscopy (AFM),[20] scanning tunneling microscopy (STM),[21] nonlinear optical probes including vibrational sum frequency generation (vSFG)[22] and second harmonic generation (SHG),[22] ambient pressure X-ray photoelectron spectroscopy (APXPS)[23] as well as measuring contact angle,[24, 25] to study the structure and dynamics of water/solid interfaces. For example, Catalano *et al.* measured the XRR spectra of water/corundum (001)[26, 27], (110)[28] and (012)[29] interfaces and analyzed the electron density profile by fitting the XRR spectra and found that water organization within 1 nm from the solid surface is affected. Experimental studies of interfacial water structure at alumina surfaces by vSFG spectroscopy have sought to understand how pH and ions affect interfacial water structures.[30-32] However, as most experiments can only provide indirect information on the structure of the surface, including the organization of the solvent and the solutes at the interfaces, researchers need models and hypotheses to interpret experimental results. However, even models supported by the highest-level calculations are not perfect.

As a result, an alternative approach, namely computational simulation, has grown in recent years (Figure 2) as computational capability has increased. Unlike indirect

experimental results that require further hypotheses for interpretation, simulations provide straight-forward microscopic structural information, i.e., the positions and velocities of each atom in every time step. With the help of easy-accessed visualization tools, researchers can observe chemical and physical processes at interfaces as easily as watching movies.[33] Computational simulations are good at handling energy-related properties, for example, calculating potentials of the mean force of adsorbed molecules, or searching for transition states during catalyzed reactions, which are difficult to measure by experimental techniques. The analysis of simulation results also becomes convenient with the help of Python, an interpreted, high-level programming language, and its libraries created by various developers.[34-36]

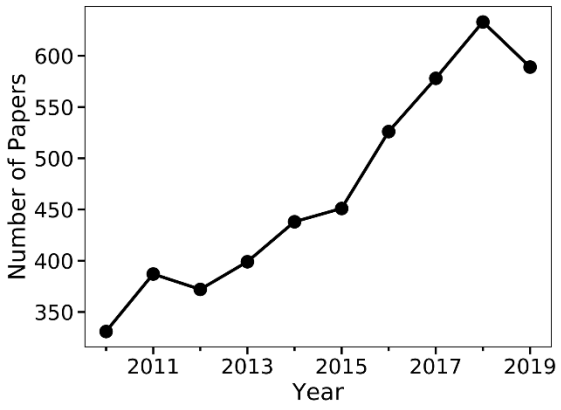

Figure 2. Number of papers published since 2010 by searching "water", "interface" and "molecular dynamics simulations" as key words. Source: "Web of Science".

Several reviews discussing MD simulations of water/oxide interfaces have been published. Bluhm *et al.*'s review about water at various interfaces, such as water/metal, water/oxide and other water/hydrophobic surfaces, featured results from both experiments and simulations.[1] Striolo *et al.* reviewed water/silica, water/alumina interfaces in 2011[37] and water/carbon interfaces in 2016.[38] YazdanYar *et al.* published a review discussing the adsorption of biological molecules at water/rutile surfaces.[39]

In this review, after a basic introduction to the principles of MD simulations we will

focus on recent studies of water/silica, water/alumina, water/TiO_2 and other mineral oxide interfaces. This review is "application-oriented", showcasing what MD simulations are able to do, what chemical scenarios can be investigated and how simulations are helpful to interpret experimental observations, such as revealing microscopic structural information of interfacial water or surfaces-adsorbed solutes, calculating the free energy of chemical reactions, assigning vibrational modes to certain species and more. At the end of the paper, we will discuss promising future directions including the application of neural-network potentials.

Principles of MD simulations

MD simulations can be used to calculate expected values of observables for macroscopic systems, given that the microscopic interactions are known. This approach relies on the ergodic hypothesis, i.e., that the ensemble average of the observations (<A>) is equal to time averages calculated using the momentum **p** and the coordinates **q** from the trajectories of simulations:

$$< A > = \int \rho(\boldsymbol{p}, \boldsymbol{q}) A(\boldsymbol{p}, \boldsymbol{q}) d\boldsymbol{p} d\boldsymbol{q} = \frac{1}{T} \int_0^T A[\boldsymbol{p}(t), \boldsymbol{q}(t)] dt \quad (1)$$

where ρ(**p**, **q**) is the probability density of state (**p**, **q**):

$$\rho(\boldsymbol{p}, \boldsymbol{q}) = \frac{e^{-\beta H(\boldsymbol{p}, \boldsymbol{q})}}{\int e^{-\beta H(\boldsymbol{p}, \boldsymbol{q})} d\boldsymbol{p} d\boldsymbol{q}} \quad (2)$$

One crucial aspect of simulations is calculating the position of all atoms as a function of time and this is done by integrating the equation of motion, typically using a numerical procedure known as the Verlet algorithm:[40]

$$r_i^{(\alpha)}(t + \Delta t) = 2 r_i^{(\alpha)}(t) - r_i^{(\alpha)}(t - \Delta t) + \frac{f_i^{(\alpha)}(t)}{m_i} \Delta t^2 + O(\Delta t^4), \quad (3)$$

where $r_i^{(\alpha)}(t)$ and $f_i^{(\alpha)}(t)$ is the alpha Cartesian component of the position and force vector, respectively, of the i^{th} particle at time t.[41, 42] Depending on how this force is calculated, simulations are referred to as classical MD or ab initio MD (AIMD).

In classical MD, electrons are not always treated explicitly and interactions between atoms can be modeled heuristically using simple analytic functions of the atoms' positions.

In non-reactive MD simulations, chemical bonds are defined in the initial configurations and cannot break or form during simulations. The potential of interactions is decomposed into bonded interaction and non-bonded interaction:[43]

$$U_{total} = U_{bond} + U_{anlge} + U_{dihedral} + U_{vdW} + U_{Coulomb}, \quad (4)$$

the first three terms are bonded interactions, including bond stretching, angle bending and dihedral torsional interactions:

$$U_{bond} = \sum_{bonds\ i} k_i^{bond}(r_i - r_{i0})^2, \quad (5)$$

$$U_{angle} = \sum_{angles\ j} k_j^{angle}(\theta_i - \theta_{i0})^2, \quad (6)$$

$$\mathrm{U_{dihedral}} = \sum_{dihedral\ m} \begin{cases} k_m^{dihe}[1 + cos(n_m\phi_m - \gamma_m)], n_i \neq 0 \\ k_m^{dihe}(\phi_m - \gamma_m)^2\ n = 0 \end{cases}. \quad (7)$$

The last two terms in equation 4 are non-bonded interactions, including the van der Waal's interactions (using Lennard-Jones 6-12 form instead) and electrostatic interactions.

$$\mathrm{U_{vdW}} = \sum_i \sum_{j>i} 4\epsilon_{ij}\left[\left(\frac{\sigma_{ij}}{r_{ij}}\right)^{12} - \left(\frac{\sigma_{ij}}{r_{ij}}\right)^{6}\right], \quad (8)$$

$$\mathrm{U_{Coulomb}} = \sum_i \sum_{j>i} \frac{q_i q_j}{4\pi\epsilon_0 r_{ij}}. \quad (9)$$

The parameters in these equations are determined empirically. As a result, the accuracy of simulations depends crucially on the choice of force field parameters. A very interesting example is water where developing accurate and convenient models is a challenge to researchers.[44] Fixed charge models, either the TIP5P model with fictitious particles modeling electrons lone pairs, or the SPC/E model with particles representing only the atoms, cannot reproduce the structure of Na^+-water complex well.[45]

Reactive force fields, including ReaxFF,[46] MEAM (modified embedded atom method)[47] or COMB (charge-optimized many-body),[48] have also been developed and widely used for water/solid interfaces.[49] The energy of ReaxFF is similar to non-reactive force fields with additional terms:

$$U_{total} = U_{bond} + U_{anlge} + U_{dihedral} + U_{vdW} + U_{Coulomb} + U_{over} + U_{specific}, \quad (10)$$

the U_{over} is penalty for overcoordination and $U_{specific}$ is usually 0 unless in special cases.[50] In ReaxFF, methods for calculating each term in eq. 10 are different from eq. 5-9; for example, when calculating bonded interactions, the concept "bond order", a differentiable property based on atoms' positions, is introduced.

In AIMD, the nuclei are still treated classically, while the forces acting on them are calculated by solving the Schrödinger equation for the electrons: $\hat{H}|\Psi>=E|\Psi>$. This cannot be solved exactly and thus most AIMD simulations are carried out at the density functional theory (DFT) level. Instead of calculating the electron ground state at every step, the Car-Parrinello (CP) approach propagates the electron orbitals by introducing a fictitious mass term:

$$L_{CP} = \frac{1}{2}\sum_{I} M\dot{R}_I^2 + \frac{\mu}{2}\sum_{i} <\dot{\Psi}_i|\dot{\Psi}_i> - E(R,\Psi) + \sum_{ij}\lambda_{ij}\left(<\Psi_i|\Psi_j> \delta_{ij}\right), \quad (10)$$

where the first term is the kinetic energy of nuclei, the second term is the fictitious kinetic energy of electrons, the third term is the Kohn-Sham equation and the last term is the orthogonality constraint of orbitals.[51, 52] When $\mu \rightarrow 0$, the CP dynamics approaches Born-Oppenheimer MD.

Historically, MD simulations were introduced in 1950; early simulations were used to study simple systems, such as hard disks (1957)[53] or Lennard Jones particles (1964).[54] The first MD simulation of bulk water was reported in 1971.[55] These seminal simulations used classical MD but those systems only contain about several hundred atoms, and were run for picoseconds due to the limitations of computational resources of that time. Nowadays, the time and length scales of classical MD simulations can reach billions of atoms and milliseconds, respectively.[56, 57] As for AIMD, CPMD was introduced in 1985;[51] due to the huge cost of electronic structure calculations, typical AIMD simulations involve hundreds of atoms and time-scales of picoseconds. Finite size effects and limited sampling of the trajectory lead to large uncertainties in the results. However, a major advantage of AIMD is that it can properly handle chemical reactions such as proton transfer,[58] catalysis[59] and water dissociation[60, 61] at interfaces.

MD simulations generate trajectories with conserved energy and momentum; if the volume of the simulation box is also fixed, the simulations are called constant-NVE

ensemble (or microcanonical ensemble). However, physical processes in other ensembles, such as NVT, NPT or even μVT are more interesting and realistic to laboratory conditions. Thanks to several algorithms, such as the Nose-Hoover thermostat[62-64] and the Martyna-Tuckerman-Tobias-Klein algorithm,[65] which make use of extended Lagrangians, simulations of NVT and NPT ensembles can be performed as well.

Water/Silica interfaces

Silicon oxide is one of the most ubiquitous minerals on the earth and its interaction with water has long been investigated by both experimental measurements and MD simulations.[66] Silica surfaces are also involved in many crucial chemical reactions that affect the earth and life,[67] such as the immobilization of CO_2[68] and the catalysis of polymerization of amino acids.[69] Silica has multiple forms, including amorphous (in many SHG and SFG experiments researchers use fused silica) and crystalline (quartz).[22] In nature, silica exists in the form of quartz, the second abundant mineral on Earth behind feldspar.[70] Although the primary component of silica or quartz is SiO_2, the surface is active to water which reacts providing surface OH groups that show acid-base behavior. Experimental SHG measurements suggest that the pK_a of 19% of the silanol groups is 4.5 and the pK_a of the other 81% is 8.5.[71] The α-quartz(001) surface is also terminated with silanol groups that show two major orientations: OH vector is perpendicular to the surface plane ("out-of-plane") or parallel to the surface plane ("in-plane").[72] In this review, we will discuss several topics about water/silica interfaces, such as ion adsorption, acid dissociation and solid dissolution.

Ion adsorption. The point of zero charge (PZC) of silica is in the pH range 2-4,[71] indicating that in ambient conditions (near pH = 7), silica surfaces will release protons and become negatively charged. The traditional EDL theories predict an interfacial electric field profile that points into the solid and exponentially decays into the solution. Interestingly, exceptions are also observed, which is not surprising because in the oversimplified EDL theories many factors such as the charge distribution at the surface and the type of ions are neglected. One example is provided by Dewan *et al*. who carried out

classical MD simulations of amorphous silica/water interfaces to understand how different charge densities, that mimic different pH environments, affect water structure and ion accumulation in the presence of NaCl or CsCl.[18] They also investigated how the charge localization (heterogeneous or uniform distribution) on the surface affects ion adsorption and water organization.[18] Simulations show that, when the surface charge is localized on SiO^- groups, specific adsorption is so strong that when the bulk concentration of Na^+ is high (0.5 M in their work), Na^+ adsorption makes the surface charge positive and reverses the water orientation (described by the opposite of water dipole) in the diffuse layer, making it point away from silica surface. In contrast, Cs^+ does not directly bind to the surface and follows the Gouy-Chapman-Stern model (GCS) model (Figure 3). Such surface charge reversal is also reported in other works and it is definitely beyond what the EDL or Gouy-Chapman-Stern model can predict.

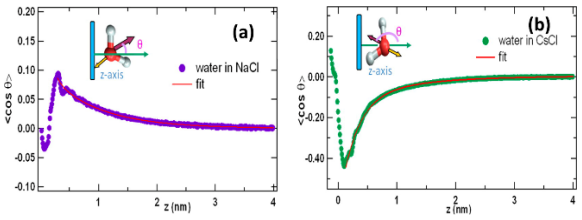

Figure 3. Influence of ions on water orientation at the water/silica interface. θ is the angle between the opposite of water dipole and silica surface normal. The silica surface is negatively charged. (a) After adding NaCl, the surface potential and <cos θ> in the diffuse layer become positive (oxygen close to the surface). (b) CsCl follows the Gouy-Chapman-Stern model. The surface potential and <cos θ> in diffuse layer remain negative (hydrogen close to the surface). Reprinted with permission from Ref 18. Copyright (2014) American Chemical Society.

Another weakness of EDL theory is that it treats the solid surface as a homogenous charged plane, which is not realistic because ions may prefer to adsorb to specific positions. For example, Hocine *et al.* calculated the potential of mean force (PMF) of cation adsorption and obtained a similar result to Dewan *et al.*,[18] finding that Li^+ has a strong

adsorption affinity but that Cs^+ is repelled by the surface.[73] The major adsorption mode for Li^+ is to directly bind to deprotonated silanol groups ($Si\text{-}O^-$) and such a binding mode is missing in EDL theories. Based on such observations, Hocine *et al.* proposed that the Stern layer is not a continuous layer but consists of some discrete contact ion pairs at the surface, e.g., $SiO^-...M^+$. As a result, predicting ion behavior simply based on its distance to the surface is not appropriate. These examples demonstrate the weakness of EDL theory at the mean field level and the necessity for more detailed structural information, which AIMD simulations are able to provide.

Interactions between the silanols that cover the surface of SiO_2 and ions are well studied for better understanding of geochemistry using both classical and ab initio MD simulations. In classical MD simulations, ion adsorption at different pH is usually studied by modifying the model of solid surface, typically changing the surface charge density or removing protons.[74-76] Not surprisingly at higher pH, when the surface contains more negative charge associated with deprotonated silanol sites, cations have higher accumulation in the Stern layer,[75, 77] and the diffusion of these ions is slower than in the bulk. Such observation could be one evidence that ions in the Stern layer are tightly bound to solid surface but are still able to move; water diffusion is also slower at the interface and even slower near deprotonated silanols.[74] In addition, ions near deprotonated silanols further decrease water diffusion.[74]

Besides classical MD, AIMD was also introduced to investigate ion adsorption at water/α-quartz interfaces. Pfeiffer-Laplaud *et al.* studied the adsorption of a single alkali ion and found that Na^+ and K^+ directly bind to the α-quartz(001) surface with partial substitution the solvation shell by surface hydroxyls, via an inner-sphere mechanism, but halides do not have any hydrogen bonds to the surface.[78] DelloStritto *et al.* investigated the acidic, neutral and basic water/quartz(101) interfaces with IA, IIA group ions and Cl^-.[79] They found that cations directly bind with the surface and behave differently from the bulk. Specifically, in the presence of a counter-ion Cl^-, the structure makers, Na^+, Mg^{2+} and Sr^{2+}, become structure breakers at the interface; the strongest "structure breaker" cations in bulk water are the strongest "structure maker" ions at the interface. These results support previous inferences from experimental data and remind researchers that simple bulk

classifications of structure maker/breaker do not always carry over to interfaces. Based on these investigations, additional questions can be asked and answered using MD simulations, such as how different surfaces and other anions affect the structure makers/breakers.

Both AIMD and classical MD predict strong Na^+ adsorption at quartz/water interfaces, which is not true for all other silica surfaces. Leung *et al.* calculated the PMF of cation adsorption with the solvation shell onto a partially deprotonated β-crystabolite(001) surface (Figure 4), a different crystal phase of SiO_2, by umbrella sampling using AIMD.[80] They found that Na^+ does not bind to that surface. Mg^{2+} can bind to the surface either directly, in the form of $Mg(H_2O)_5(SiO^-)$, or via its intact hydration shell. Direct binding is more favored by about 0.2 eV. Interestingly, the surface SiO^- will grab a proton from the hydration shell of Cu^{2+}, forming a $Cu(OH^-)(H_2O)_3$ complex ion. As a result, the authors proposed that in future CMD simulations, a Cu^{2+}-OH^- based model should be used. Although AIMD is much more expensive than classical MD, it is useful and necessary if the hydration shell of ions is able to release protons.

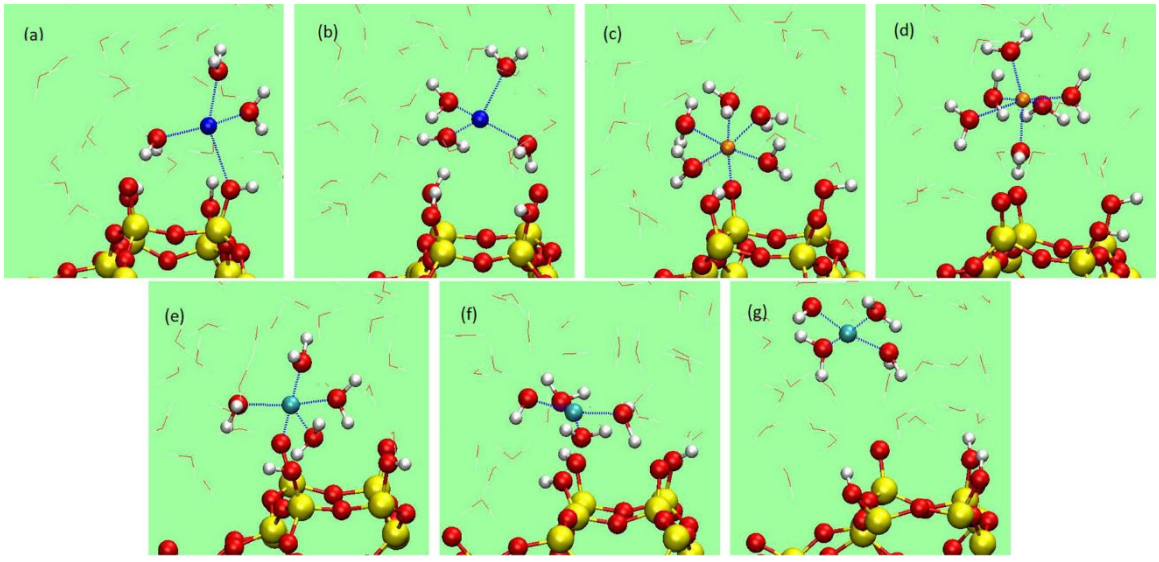

Figure 4. Different ion binding modes between ions and the β-crystabolite(001) surface. Yellow, red, white, blue, orange and green balls represent Si, O, H, Na, Mg, Cu atoms(ions), respectively. a) and b) Na^+ binding modes, c) Mg^{2+} directly binds to the surface, d) Mg^{2+}

with completed hydration shell. e) Cu^{2+} binds to the surface, f) and g) $Cu(OH^-)(H_2O)_3$ complex ion. Reprinted with permission from Ref 80. Copyright (2018) American Chemical Society.

Adsorbed cations affect surface silanol properties as well. In the presence of cations, the intra-surface H-bond network is weakened, accelerating the switching of silanols between "in-plane" and "out-of-plane" modes, which is rarely observed at neat interfaces on typical AIMD timescales.[78] In their later work, Pfeiffer-Laplaud *et al.* studied a cation-anion solvent separated pair at the same surface and found that the orientation and bond-length of the surface OH groups are more affected and that intra-surface H-bonds are more weakened by such an ion-pair than by a single ion.[81]

In addition to the works mentioned above, there are other studies investigating ion adsorption at interfaces,[82] including organic molecule ions.[83] Other than simulations with only one type of ion-pair, Döpke *et al.* carried out simulations of water/silica interfaces with the NaCl-$CaCl_2$ mixture and found that Na^+ shows more preferential adsorption to silica surface than Ca^{2+} because Na^+ has a less tight hydration shell and the surface structure adsorption site does not match the hydration shell of Ca^{2+}.[84]

Acid dissociation. There are several interesting pK_a related questions about interfaces: how do surfaces affect the water pK_a, what is the pK_a of the surface OH groups, how do adsorbed solutes affect the surface pK_a and how do surfaces affect the pK_a of solutes at the interface. Answering such questions is quite challenging due to the complicated environment of interfaces and even the value of the water pK_a at water/air interfaces, possibly the simplest surface, is still controversial because some MD simulations show that water/vapor interfaces are acidic,[85-88] but the opposite result that such interfaces are basic has also been reported.[89-91] Nevertheless, significant advances related to the acid/base chemistry of water/silica interfaces have been made with the help of MD simulations.

The simplest example is the pK_a calculation of hydroxylated α-quartz(0001) surface OH groups as there is only one type of silanol with two orientations; "out-of-plane" silanols

are reported to have a lower pK_a (5.6) than "in-plane" silanols (8.5).[92] When an alkali-halide ion pair is placed at the interface, the cation will bind to the oxygen atom of the silanols, stabilize the OH bond and prevent deprotonation.[93]

The pK_a of amorphous silica silanols is more complicated. Using free energy perturbation, Pfeiffer-Laplaud *et al.* identified and calculated the pK_a of 4 types of silanols on silica surfaces: isolated, H-bonded, vicinal and geminal; the terminal group of the former three is SiOH and that of the last one is $Si(OH)_2$ (Figure 5).[94] They found that convex geminal and vicinal silanols have strong acidity with a pK_a value about 2~3, while the isolated and concave germinal species have much higher pK_a (9~10). Such bimodal acidity has already been observed by SHG experiments[71] and with the help of AIMD simulations researchers can identify its microscopic origin.

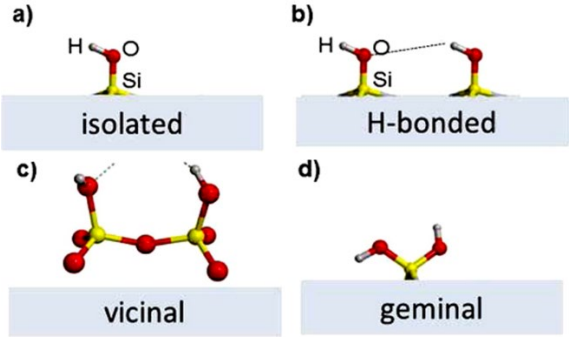

Figure 5. Classification of silanols on amorphous silica surfaces. "Isolated" silanols are not hydrogen bonded with other silanols; "vicinal" silanols share one common oxygen atoms and "geminal" silanols have two OH groups connected with one silicon atom. Reprinted with permission from Ref 94. Copyright (2015) American Chemical Society.

A more interesting question, perhaps, is understanding how interfacial environments affect the acid/base chemistry of species nearby, such as the pK_a of a solute molecule. This topic has a close relationship to heterogeneous catalysis, including amino acid condensations reactions near water/silica interfaces. Parashar *et al.* constructed water/α-quartz(0001) interfaces with two pyruvic acid molecules (Figure 6), one at the surface in a protonated state (HA) and the other one in the bulk in the form of a deprotonated ion (A^-).[95]

Using the free energy perturbation method,[96] they calculated the Helmholtz free energy difference, to move the proton from the HA molecule at the surface to the A^- in the bulk. They found that at the interface, the acidity increased due to the stabilization of A^- by surface OH groups and interfacial water. The design of this work is ingenious since it only calculated the pK_a differences of an acid at the surface and in the bulk, instead of calculating absolute pK_a values.

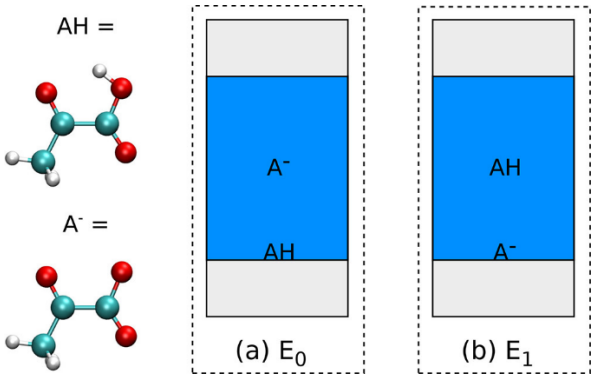

Figure 6. The calculation of ΔpK_a of pyruvic acid at an interface. The structures are the protonated acid (HA) and the deprotonated ion (A^-). (a) Initial state with HA at the surface and A^- in the bulk. (b) Final state with A^- at the surface and HA in the bulk. Reprinted with permission from Ref 95. Copyright (2018) American Chemical Society.

Simulations of vibrational spectra. Besides analyzing chemical structures and calculating free energies, MD simulations can also help interpret experimental vibrational spectra, such as IR and Raman. For water/solid interfaces, nonlinear optics, such as vSFG and SHG are intensively used because they are sensitive to the non-symmetric environment that interfaces naturally possess.[22] Usually, vSFG spectra can be decomposed into $\chi^{(2)}$ and $\chi^{(3)}$ contributions, arising from interfacial region and bulk water, respectively.[97] The $\chi^{(2)}$ contribution is determined from the autocorrelation function of the molecular dipoles and polarizabilities.[98]

Since the silica surface is charged at pH 7, it has been widely used as a model of charged surfaces by combining MD simulations and experiments. Gaigeot *et al.*

calculated the vibrational density of states of interfacial OH groups (both from water and silanols).[72] They found that the H-bonds that water molecules donate to the "in-plane" silanols (OW-HW…OSi) are weak and contribute to vibrations in the 3300-3600 cm^{-1} range.[24] By carefully calculating the vSFG spectra of water in different layers close to interface, Pezzotti *et al.* proposed a new definition of the electric double layer. To be specific, the boundary of the Stern layer (in their work it is called the "binding interfacial layer", BIL) can be identified because its properties, such as water density profile and hydrogen bond profile, are distinct from bulk water and their vSFG spectra are surface type dependent. However, the hydrogen bond structure in the diffuse layer behaves similarly to bulk water except for the net orientation caused by the interfacial electric field. As a result, the vSFG signals of water in diffuse layers of water/quartz and water/air interfaces are similar.[99] This work is a demonstration that water in the diffuse layer follows the assumptions of EDL theories that water is aligned by a homogenous electric field. It will interesting to see whether the diffuse layer of other aqueous interfaces follow this pattern.

The combination of vSFG and simulations provides detailed microscopic structural information and is helpful for researchers to understand the behavior of water interfaces, not limited to water/silica interfaces.[10098, 101-103] One interesting question at charged water/solid interfaces is the separation of the second-order ($\chi^{(2)}$) and the third-order ($\chi^{(3)}$) contributions of vSFG spectra; the latter one comes from the static electric fields of charged interfaces. Several experimental attempts for such separation have been reported by changing the pH or ion concentrations.[104, 105] However, those methods are not perfect because the surface charge state and water structures in the compact layer are also affected, leading to the change of $\chi^{(2)}$ signal as well. By designing MD simulations containing water between two charged silica surfaces, modifying the charge density on the surfaces and calculating how the water responded to this electric field, the corresponding $\chi^{(3)}$ contribution could be extracted.[97] This procedure helps researchers understand the $\chi^{(3)}$ effects near charged water/solid interfaces and such a decomposition can be used to extract the $\chi^{(2)}$ component from vSFG spectra to investigate the interfacial structure.

The preceding discussions focused on perfect solid silica surfaces. However, water/silica interfaces are not always stable, especially in high pH solutions,[106] and the

dissolution (or degradation) can also be studied by MD simulations.[107] Using both classical MD with ReaxFF and AIMD simulations, Rimsza *et al.* calculated the first step of silica dissolution, the breaking of strained silica and the formation of unstrained silica (Figure 7).[108] First, a water molecule adsorbs onto an external Si atom of a strained silica site and releases a proton (Figure 7 a-c); next, another proton comes to the bridging oxygen, leading to the rupture of the Si-O bond (Figure 7 d, e). Simulations also provide the time scale of such reactions.[108] In their later work, they also studied the evolution of the silica gel region between bulk water and bulk silica solid.[109] Since the dissolution of silica is usually neglected when studying water/silica interfaces, these works provide useful information regarding solid dissolution and may help researchers improve their design of experiments to avoid/promote silica dissolution.

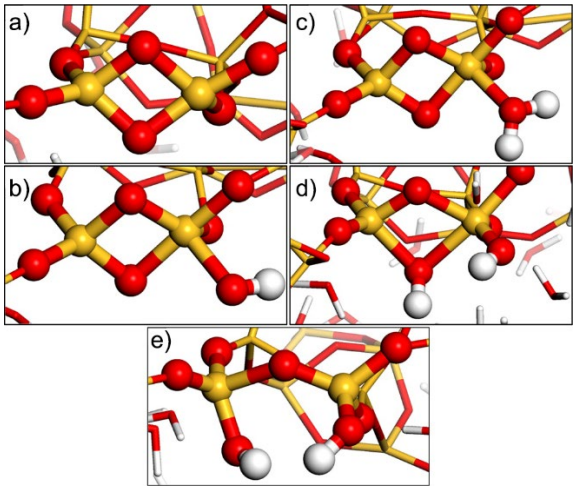

Figure 7. The mechanism of how strained silica become unstrained silica. (a) Strained silica, the initial state. (b-d) Intermediate defect structures. (e) unstrained silica, the final state. Reprinted with permission from Ref 108. Copyright (2016) American Chemical Society.

Water/Alumina (Aluminum Oxide) Interfaces

Aluminum is the third most abundant element on earth after oxygen and silicon, and mostly exists in the form of oxides due to its high reactivity. However, water/alumina

interfaces are less understood than water/silica interfaces in spite of their important roles in ion adsorption and catalysis. Alumina has wide industrial applications,[110] for example, γ-Al_2O_3 can be used as the support of catalyst.[111, 112] We focus on α-Al_2O_3 because it is the most thermodynamically stable phase; the coordination number of aluminum is 6 in bulk α-alumina, forming an octahedron and that of oxygen is 4, forming a tetrahedron. The fully hydroxylated, charge neutral water/α-Al_2O_3 interface has been studied by several groups focusing on interfacial water structures and dynamics.[26, 37, 77, 113, 114] Particularly, the vSFG of water/alumina (0001) and $(11\bar{2}0)$ interfaces under various pH in the presence of monovalent ions has been measured to estimate the structures of interfacial water and hydrogen bonds.[30, 32] The α-alumina(0001) surface is flat, containing only one type of aluminol Al_2OH, but the $(11\bar{2}0)$ surface is rough and complicated, containing AlOH, Al_2OH and Al_3OH groups with different heights (Figure 8).

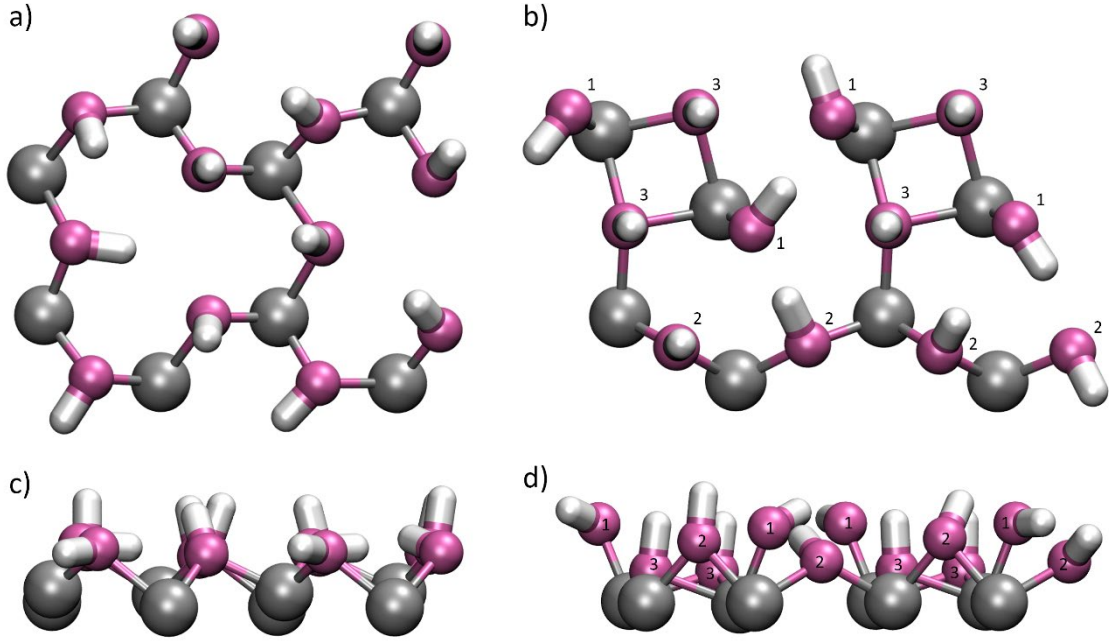

Figure 8. The structure of α-alumina (0001) and $(11\bar{2}0)$ surfaces. Water is not shown for clarity and gray, purple and white color represent aluminum, oxygen and hydrogen atoms, respectively. The top two figures show the top view of (0001) (a) and $(11\bar{2}0)$ (b) surfaces; the bottom two show the side view of (0001) (c) and $(11\bar{2}0)$ (d) surfaces. The

numbers in figure (b) and (d) represent how many aluminum atoms are connected with each oxygen, i.e., the 'x' of Al_xOH. The figures only show one simulation box so the periodic boundary condition is broken.

The impact of ions on water/alumina interfaces has also been investigated by MD simulations. Wang *et al.* observed unusual ion adsorption onto the water/α-alumina(0001) interface, due to the special pattern of surface OH groups.[115] By comparing the adsorption free energy, they found that in simulations of a single ion, Na^+ has a stronger affinity to the solid surface than halides; in simulations of finite concentration solutions, the affinity of Na^+ decreases and that of halides increases, indicating that adsorbed Na^+ ions promote halide ion adsorption. The adsorbed excess Na^+ can increase water polar orientation and change its dipole direction. As discussed before, such effects cannot be predicted by EDL theories. In addition, ignoring the Al-O-H angle bending term in the potential could cause the underestimation of ion adsorption (Figure 9).[116] Recently those terms in ClayFF have been improved, leading to a distribution of the orientations of surface OH groups that is in better agreement with DFT simulations.[117]

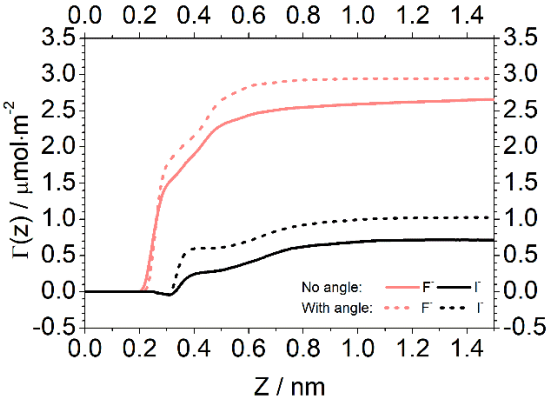

Figure 9. Surface excess ions per unit surface area, Γ(Z), profile of F^- and I^- near the water/α-alumina(0001) interface. The counter-ion is Na^+. Comparing to results with the bending potential, simulations without it underestimate ion adsorption. Reprinted with permission from Ref 115. Copyright (2019) American Chemical Society.

AIMD simulations are also applied to calculate and analyze the vibrational spectra of alumina/water interfaces. DelloStritto *et al.* successfully reproduced the features observed in experimental spectra of the water/α-alumina(0001) interface, namely a peak centered at 3150 cm^{-1} and a higher peak around 3450 cm^{-1},[118] which were previously assigned to water with different coordination numbers.[119] However, both water and "in-plane" aluminols contribute to the 3400 cm^{-1} peak and the latter is usually ignored. Further calculation of the vibrational density of states indicates that "out-of-plane" aluminol vibrations are at higher frequency, between 3600 and 3800 cm^{-1}, unlike the α-quartz(0001) surface whose vibrational density of states of both "in-plane" and "out-of-plane" silanols overlap in a wide region 3000-3800 cm^{-1}.[72] Later, DelloStritto *et al.* compared the performance of several popular exchange and correlation functionals, including PBE, PBE with Tkatchenko−Scheffler correction (PBE-TS), revised PBE and SCAN meta-GGA functionals; they found that revised PBE has poor performance in reproducing experimental interfacial water structures and vSFG spectra, even though it does well for the water/vapor interface.[101] Spectra predicted by revised PBE show too much blueshift whereas spectra from PBE or PBE-TS have stronger intensity in the low frequency region, indicating that they predicted an overstructured interfacial water as they did for bulk water.[120, 121] The meta-GGA SCAN functional,[122] which has provided more accurate description of the structure,[123] dynamics,[124] IR spectra[125] and pK_a[126] of bulk water as well as the solvation structure of Cl^-,[127] outperforms PBE-TS, giving the best interfacial structure, dynamics and vSFG spectra, demonstrating that the SCAN functional can describe interfacial water and the solid surface well at the same time (Figure 10).[121] Interestingly, the spectrum of the α-alumina$(11\bar{2}0)$/water interface shows more redshift than the less corrugated (0001) interface while water at the (0001) interface has longer H-bond lifetimes and a larger order parameter. As a result, concepts such as "strong H-bonded", "ordered", "redshifted", "ice-liked" are correlated, but they are not equal and observing one behavior does not guarantee the others. Thus, we should be careful when using these concepts.

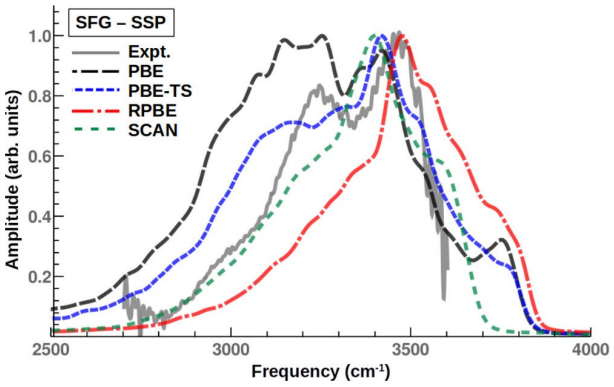

Figure 10. Comparison of vSFG spectra of the water/α-alumina(0001) interface from experiments and AIMD simulations. The spectrum predicted by SCAN agrees best with experiments in this work. Spectra from PBE or PBE-TS overestimate intensities at low frequency while features at low frequency are missing in RPBE. Reprinted with permission from Ref 121. Copyright (2019) American Chemical Society.

The vSFG of the alumina(0001) surface was also calculated by Melani *et al.* with simplified parametrized velocity-velocity autocorrelation function methods and they proposed a similar interpretation as DelloStritto *et al.*.[128] These works provide a well-defined paradigm to analyze vSFG spectra using AIMD simulations: running simulations with advanced density functionals, such as the SCAN functional, then calculating the vSFG spectra of the system and its components. By carefully comparing simulation results and experimental measurements and assigning experimental peaks, more microscopic structure information can be revealed to advance our understanding of water/solid interfaces.

Besides vSFG, XRR is also used to study the water/α-alumina(0001) interface. Effective electron density can be obtained by fitting the XRR and compared with that calculated from MD simulations.[26, 129] Experimental and simulated results were qualitatively similar, but quantitatively different (Figure 11), indicating that an improvement of current density functionals is still required, especially the ones with moderate cost that could be used for AIMD simulations.[26, 129]

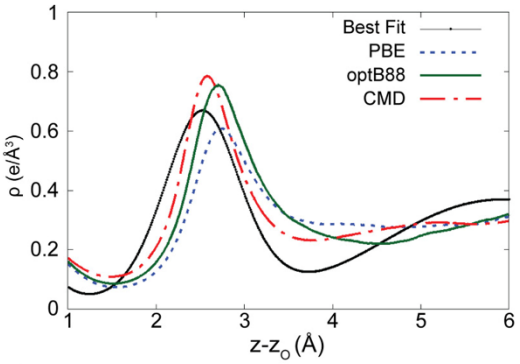

Figure 11. Comparison of experimental and simulated electron density profiles of the water/α-alumina(0001) interface. "z-z0" is the distance of Z direction (surface normal) and 0 is set to the surface outmost oxygen plane. Black curve ("Best Fit") is the fitted electron density from XRR measurements. Blue ("PBE") and green ("optB88") curves are results directly calculated from AIMD simulations using different functionals. Red curve ("CMD") is results from classical simulations. Reprinted from Ref 129.

As mentioned above, alumina draws less attention than silica and many important questions still puzzle researchers. One example is the pK_a of the octahedral Al_2OH group, which is the only type of hydroxyl group on the alumina(0001) interface, reported as 16.6 by one source,[72] while the pK_a of water/gibbsite(0001) reported as 22,[130] both determined using the BLYP functional. Gibbsite is one polymorph of $Al(OH)_3$ whose (0001) surface has similar octahedral Al_2OH groups as alumina(0001). However, experimental measurements using potentiometric titration report the pK_a of Al_2OH as 12.5.[131] The reason of such discrepancy between experiments and simulation is unknown and requires more investigation. What is more, a bigger problem is that the experimental pK_a is smaller than that of water, indicating the surface will deprotonate in basic solutions but all simulation results shows the surface will not.[130] Interestingly, hematite(0001) surface is similar to alumina (0001) and the predicted pK_a of Fe_2OH by AIMD is 21.7, comparable with Al_2OH, but much higher than the value predicted by the valence bond model (about 12),[132] but the pK_a of SnO_2 is consistent with experimental PZC measurements.[133] Understanding disagreements between simulations and experimental measurements is

crucial to model the interface in acidic or basic solutions because the surface protonation state, surface charge density and interfacial water orientation are mainly determined by the surface pK_a.

Water/TiO_2 interfaces

Titanium oxide is widely used in white pigments, photocatalysts, electrochemical devices and biocompatibility materials.[134] Several reviews focusing on TiO_2 surfaces or water/TiO_2 interfaces have been published in the past few years.[135, 136] The common TiO_2 forms occurring in nature are rutile, anatase and brookite, and rutile(110), its most stable facet, has been the most widely studied.[137]

Water adsorption. The simplest scenario related to water/TiO_2 interfaces is the pure water adsorption onto the perfect, defect-free solid surface, which has been studied by the combination of experimental phase-sensitive vSFG and AIMD simulations. Both Hosseinpour *et al.*[138] and Andrade *et al.*[139] observed a positive peak at 3100 cm^{-1}, assigned to "physisorbed" water that donates a strong H-bond to the surface, and a negative peak at 3400 cm^{-1}. However, the origin of feature at 3400 cm^{-1} is under debate. Hosseinpour *et al.* proposed the concepts "chemisorbed" and "physisorbed" water; the former is dissociated water forming a covalent OH bond with the surface five coordinated Ti atoms and the latter remains intact water molecule. In Hosseinpour *et al.*'s work, water at 3400 cm^{-1} is assigned to "chemisorbed" water molecules,[138] while in Andrade *et al.*'s work, after water dissociated adsorption, the signal at 3400 cm^{-1} decreased comparing to non-dissociated simulations, because such dissociation perturbed water in the first layer.[139]

The 'chemisorbed' water is also reported in other simulations of water/anatase(101) and water/rutile(110) interfaces using a reactive force field.[140] Water first contacts with 5-coordinated Ti atoms, dissociates leaving hydroxyl groups that form $Ti_{5c}OH$ like structures. The resulting H^+ moves to the nearest 2-coordinated surface oxygen (O_{2c} for anatase and O_b for rutile, Figure 12). All O_{2c}/O_b sites are covered by H^+ but only half of the Ti_{5c} sites are terminated by OH^-. The coverage of Ti_{5c} for anatase(101) is higher than that of rutile(110), leading to a higher positive surface potential of rutile(110) than that of

anatase(101). The diffusion constant of water near those interfaces is about 2 orders of magnitude slower than the bulk, indicating strong water-interface interactions but the average interfacial hydrogen bonds strength and lifetime do not increase significantly. One weakness of this simulation is that the IR spectrum predicted by ReaxFF is less accurate than expected, indicating that fast classical simulations may not be able to reproduce all the properties of the studied systems.

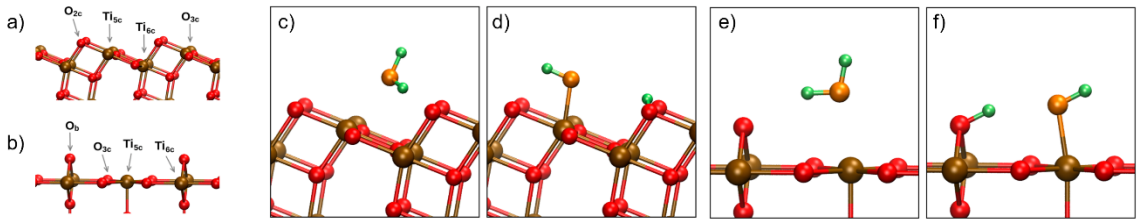

Figure 12. Water dissociated adsorption on TiO_2 surfaces: (a) the structure of anatase(101) and (b) rutile(110) surfaces with atom labels; (c) before and (d) after water dissociation at the anatase(101) surface; (e) before and (f) after water dissociation at the rutile(110) surface. Reprinted with permission from Ref 140. Copyright (2017) American Chemical Society.

Water dissociation is also observed at the brookite (210) interface and interestingly, ions, such as K^+ and Cl^-, are found to promote water dissociation and increase surface hydroxylation, that is, more than 30% of surface groups are hydroxylated when KCl is present, comparing to less than 20% in pure water.[141] Previous research has shown that the hydroxylation of the TiO_2 anatase surface can enhance the photocatalytic efficiency for water splitting.[142] Since the carbonate ion can enhance hydrogen evolution at the $K_4Nb_6O_{17}$ surface,[143] it will be exciting if ions can further increase the photocatalytic efficiency on TiO_2 or other surfaces.

According to the works discussed above, simulations have enabled a clearer picture about the microscopic nature of (pure) water/TiO_2 interfaces to emerge. Some TiO_2 surfaces are superhydrophilic due to strong interactions with both “physically” and “chemically adsorbed interfacial water. The chemical adsorption, or dissociated adsorption of water, can also happen at water/TiO_2 interfaces, making the surface OH

terminated. Since electrochemical catalysis is one of important applications of TiO_2, preliminary knowledge of water adsorption on the TiO_2 are essential to inspire better materials design.

Electrochemical applications. Since 1972, when Fujishima and Honda discovered the photocatalytic power of TiO_2,[144] designing high efficiency materials for water splitting or hydrogen generation to overcome the energy crisis has become one of the most popular areas in scientific research. Many MD simulation papers related to this topic have been published in recent years, mainly focusing on the oxygen evolution half-reaction because oxygen evolution reaction (OER) is the rate-determining step at TiO_2 interfaces.[145, 146] Valdés *et al.* proposed the following mechanisms from AIMD simulations of the water/rutile(110) interface for water oxidation, containing four sequential proton-electron transfer (PET) steps at water/anatase(101) interfaces in the presence of surface-trapped photoexcited holes:[146]

$$*OH_2 + h^+ \rightarrow *OH + H^+ \quad (11)$$

$$*OH + h^+ \rightarrow *O + H^+ \quad (12)$$

$$*O + H_2O + h^+ \rightarrow *OOH + H^+ \quad (13)$$

$$*OOH + h^+ \rightarrow O_2 + H^+ \quad (14),$$

in which the first step is the most difficult. Recently, Li *et al.* investigated water oxidation on the anatase(101) surface using the hybrid density functional PBE0.[147] Based on the mechanism above, the authors find that the first step requires water adsorption at Ti_{5c} site and releases a proton to create an *OH radical.[147] Next, the proton in *OH radical leaves, the *O and a surface oxygen together form a bridging peroxo dimer $(O_2^{2-})_{br}$. The last two steps involve a concerted two-electron-transfer pathway, instead of a nucleophilic attack from water that was reported at a rutile surface.[148-150] The authors also state that the lower probability of the two-electron-transfer is the reason for the lower OER performance of anatase compared to rutile.

Stecher *et al.* calculated the free energy barrier for water oxidation at the rutile(110) interface using QM/MM techniques.[151] QM/MM can provide better sampling and overcomes some infinite-size effects due to the limited scale of AIMD simulations.

Another improvement of this work is that energy gap is selected as the reaction coordinate instead of common geometric coordinates. The results show that the free energy barrier is 0.2-0.25 eV higher than the rutile band gap, depending on the orientation of one water molecule. Those numbers indicate that OER reactions are not able to happen near the perfect rutile(001) interface. An alternative hypothesis is that defects on the surface promote water dissociation, which has been observed on the rutile(110) surface.[152] Excess electrons can be generated from the defects and their behaviors have been investigated by Selcuk *et al.*.[153] They found that an excess electron at the water/anatase(101) interface can be trapped, forming a stable Ti^{3+}-$O_{br}H$ complex, which facilitates reduction reactions. However, the (001) surface repulses electrons and oxidation reactions are favored. These results are in good agreement with photoemission spectra and the authors proposed that catalytic activity can be tuned by optimizing the ratio of anatase (101) and (001) surfaces. Since catalysis at TiO_2 surfaces is still a hot area, simulations can be used to reveal the mechanisms by quantifying the free energy along reaction coordinates or analyzing the electron behaviors.

Biomolecule adsorption. Due to the biocompatibility and biosafety of TiO_2, its applications as implant materials or biosensors are of great interest.[39, 154] It is necessary to investigate the interaction between the solid surface and small biomolecules since they are ubiquitous in human beings and such interactions could be harmful to patients. Amino acids or short peptides can be chosen as model molecules since they can be a mimic of proteins, the molecules of life.

YazdanYar *et al.* studied adsorptions of several single amino acids (Ala, Asp, Lys, Arg, Leu, Ser) on the negatively charged rutile(110) surface.[155] Using well-tempered metadynamics, they calculated the PMF with respect to two collective variables, the distance between the solid surface and center of amino acids' backbone or side group. Such separated collective variables help the interpretation of molecule adsorption. All six amino acids can be adsorbed by the negatively charged surface via their backbone, irrespective of their side group. It is not surprising that Arg and Lys, whose side chains are positively charged, can also be adsorbed via their side chains.

Ions can also affect biomolecule adsorption. For example, Zheng *et al.* studied tripeptide (Pro-Hyp-Gly) adsorption on rutile(110) and found that Ca^{2+} does not affect the tripeptide adsorption on the neutral surface, but leads to a strong interaction with both the negatively charged surface and COO^- groups, making the tripeptide indirectly bind with the surface and finally transform to directly bind via the COO^- group.[156] In practice, using small model molecules for studying biomolecule adsorption is a preliminary but very important attempt because a simulation containing a whole protein and solid surface is computationally costly to carry out and analyze.

The next step can be to extend to simulations with biomacromolecules and a wider range of material surfaces, which can be used to predict the properties of designed biomaterials. For example, the interaction between the protein BMP-2, a growth factor for bone regeneration, and pure, OH-terminated or phosphite-modified rutile(110) and anatase(101) surfaces have been investigated and the phosphite-modifed TiO_2 surfaces have revealed two effects on promoting bone regeneration: 1) enhancing the adsorption of the BMP protein, 2) changing the orientation of BMP, making its wrist epitope point outwards and bind to BMP receptor type-I on cell membranes (Figure 13, c and f).[157] Since interactions between proteins and oxide surfaces can affect physiological functions of implanted materials and because oxide surfaces can be modified by surface treatment, e.g. grafting functional groups or polymers, taking advantage of MD simulations can definitely lead to better design of biomedical materials by predicting their interactions before clinical assays.

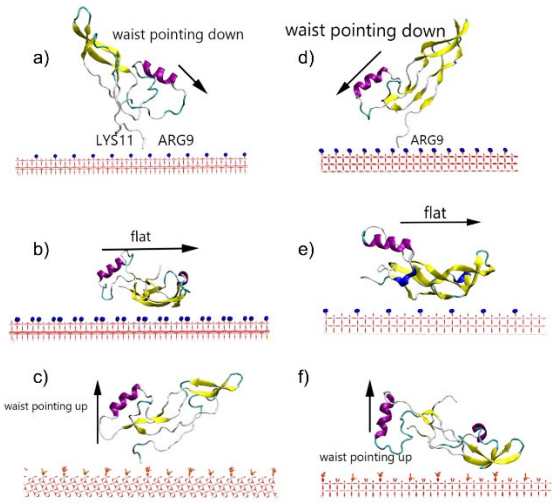

Figure 13. BMP-2 adsorption modes at different water/TiO_2 interfaces. Purple color highlights the wrist epitope, which shows different orientations depending on the surface terminated groups. a), b) at the OH-terminated anatase(101) surface, the wrist epitope either points down or stays flat, c) at the phosphite-terminated anatase(101) surface, the orientation of the BMP-2 changed and its wrist epitope points up. It also points down (d) or stays flat (e) at the OH-terminated and points up (f) at the phosphite-terminated rutile(110) surface. Reprinted with permission from Ref 157. Copyright (2018) American Chemical Society.

$(SiO_2)_x \cdot (Al_2O_3)_y \cdot (MO_z)_m$

Besides silica and alumina, aluminosilicates are a significant component of the earth's crust.[158] Here, in order to avoid the complexity of the definition, we would like to discuss minerals containing silicon, aluminum and oxygen together.

Kaolinite ($Al_2O_3 \cdot 2SiO_2 \cdot 2H_2O$), an essential material for ceramic industries, is able to adsorb cations,[159] including the nuclear waste Cs^+.[160] Interestingly, Zeitler *et al.* found that ion adsorption affects the uptake of a negatively charged crude oil model molecule at the edge kaolinite (010) surface. Although the number density of adsorbed Ca^{2+} and Na^+ are similar, Ca^{2+} enhances the uptake of oil molecules whereas Na^+ is not able to do so, providing theoretic explanation why injecting low salinity fluids can increase oil

717 detachment from rocks to improve hydrocarbon recovery.[161]

718 Mica is a general name for a group of layered, sheet-like oxides of aluminum and
719 silicon, one of which is muscovite whose formula is $KAl_2(AlSi_3)O_{10}(OH)_2$. The
720 water/muscovite(001) interface has a flat cleavage surface and has been widely
721 investigated by various experimental methods such as XRR and AFM. To better interpret
722 AFM measurements of water/muscovite interfaces, Kobayashi *et al.* simulated AFM data
723 by classical MD simulations.[162] After decomposing the measured force, they found that
724 the surface first hydration layer (the water layer nearest to the solid) contributes most of
725 the force of adhesion. Since the muscovite surface itself contains ions, an interesting
726 question is how ions on the surface and ions in water affect each other. The muscovite
727 (0001) lattice is hexagon-like and a K^+ sits in the center of each hexagon but under certain
728 conditions, K^+ can be replaced by other cations. Later, they carried out MD simulations
729 with other ions in group IA and IIA and found three binding types between cations the
730 surface: at the center of hexagon sites (IS1), on top of Al (IS2) or out from the surface (OS)
731 and the formation of IS1 and IS2 is highly dependent on the charge density of the adsorbed
732 ions.[163] The charge state of mica solid also affects cation adsorption; Jia *et al.* compared
733 Na^+, K^+ and Cs^+ adsorption on mica surfaces with various charge densities and found that
734 ion adsorption followed the sequence $Na^+ > K^+ > Cs^+$ at the low charge density surface
735 (0.16 $C \cdot m^{-2}$ and lower) and $Cs^+ > K^+ > Na^+$ at the high one (0.24 $C \cdot m^{-2}$ and higher).[164]
736 Mica continues to be an important model surface, for understanding ion adsorption.
737
738 **Applications of simulation with other interfaces**

739 **Heterogeneous catalysis.** By choosing reaction coordinates carefully, the potential
740 energy surfaces (PES) can be calculated using MD simulations and a trajectory of how
741 reactants become products could be identified from the PES plot. The highest point on
742 the reaction path is the transition state and its energy difference from the reactants is the
743 reaction barrier. The protocol is successfully used to study many chemical processes,
744 including catalysis by metals.[165]

745 One example we will discuss in this review is the spontaneous water dissociation at
746 the water/CeO_2(111) interface.[166] Farnesi Camellone *et al.* designed a CeO_2 surface with

747 a Pt_6 cluster on it. They found that after a proton transfer to the CeO_2 surface, the resulting
748 OH^- binds to a Pt site instead of the Ce site.[167] More interestingly, the dissociated water
749 molecule can either directly dissociate at the Pt cluster, or away from the cluster; in the
750 latter case, the resulting OH^- is quickly transferred to the Pt cluster via the Grotthus-like
751 proton transfer mechanism. The solvent water can help charge transfer, making an
752 electron of OH^- move to solid Ce(IV) atom, reducing it to Ce^{3+}.[168] Such charge transfer
753 cannot happen if no Pt cluster is on the solid surface. Similar structures, such as gold
754 nanoparticles (AuNP) on TiO_2 surfaces are predicted to catalyze O_2 splitting for the
755 oxidation of alcohol.[169] Muñoz-Santiburcio *et al.* compared the reaction mechanisms in
756 gas phase and liquid phase to investigated how solvent water molecules enhanced the
757 catalysis efficiency.[169] In the gas phase, the proton of the reagent, Methanol, donates its
758 hydroxyl proton to surface preadsorbed dissociated O_2 and an aliphatic hydrogen moves to
759 the AuNP in the form of hydridic H^-. The concerted mechanism in the gas phase requires
760 that all charge transfer happen at the same time, as a result, substrate needs to co-adsorb to
761 O_2 and AuNP simultaneously. However, in the liquid phase, the reaction is stepwise,
762 decoupled in time and space. After donating the hydroxyl proton by Grotthuss
763 mechanism to surface dissociated O_2, the intermediate is stable and has more opportunity
764 to adjust its configuration until an aliphatic hydrogen moves to the AuNP. In addition, in
765 the presence of liquid water, the AuNP contains more charges that are stabilized by water
766 solvent molecules, which can enhance the activation of surface adsorbed O_2 and the overall
767 catalytic efficiency. This suggests that doped water/solid interfaces are promising
768 catalysts.
769 However, water/solid interfaces are not always good for catalysis. One example is
770 acetic acid ketonization on the $ZrO_2(\bar{1}11)$ surface. By comparing the reaction paths in
771 the gas phase and in aqueous solution, Cai *et al.* observed a lower reaction rate at the
772 water/ZrO_2 interface than at the vapor/ZrO_2 interface because at high water coverage,
773 surface sites are occupied and substrate accessibility decreased.[170] Nevertheless,
774 water/solid interfaces are very promising systems for catalysis, especially when doped by
775 nano-scale clusters. It can be expected that the demand for such catalysts will keep
776 increasing and their careful design is of vital importance. As a result, AIMD simulations

can be useful to predict and prescreen "future" materials.

Prebiotic peptide formation. The polymerization of small biomolecules, such as amino acids or nucleotides, forming proteins or nucleic acids, is believed to be a fundamental process in explaining the origin of life.[69] Amino acids condensation is not favored in bulk water but mineral surfaces, such as silica, are able to catalyze the reaction.[171] Besides silica, using $Mg_3Al(OH)_8^+$ as a model of layered double hydroxides, which were common in early earth, Erastova *et al.'s* MD simulations demonstrated how the mineral surface helps amino acids adsorption and alignment, as well as how wetting-drying cycles help peptide bond formation.[172]

MD simulations of interfaces using neural network potentials

MD simulations are based on a mapping between any given molecular configuration and energy; this map is used to calculate forces and thus to generate a time-evolved configuration after integration of the equations of motion. The most accurate methods are those obtained from post-Hartree-Fock methods, based on quantum mechanics and a numerical solution of the Schrodinger equation. This level of accuracy is required to make reliable predictions on, for instance, molecular configurations. However, these AIMD simulations are very time-consuming even when DFT is used for solving the electronic structure problem. In classical MD simulations, complex interactions between atoms are phenomenologically captured by analytic functions of the atomic coordinates, such as bond lengths, bond angles, dihedrals and charges on atoms. This highly approximate approach is very useful because of the relatively low computational cost. However, due to the limitations of the mathematical form of force fields and the empirical process of optimally parametrizing them, the accuracy of classical MD simulations is not guaranteed and, perhaps most critically, it is difficult for classical MD to handle chemical reactions.

An alternative approach to empirical force-fields that is gaining increasing popularity is based on neural networks potentials (NNPs). This family of algorithms, traditionally employed in applications such as face recognition, self-driving cars and decision-making,

807 can be used to calculate energies or forces for MD simulations directly from the chemical
808 structures after proper training.[173] NNP-MD simulations have the disadvantage that the
809 energy function cannot be easily interpreted in terms of intuitive physical concepts such as
810 bond lengths, angles, etc. However, its computational cost is much lower than that of
811 AIMD. As a result, NNP-MD can also reach AIMD-level accuracy but the scale can be
812 increased to thousands of atoms for several nanoseconds (an improvement of two orders
813 of magnitude both in length- and time-scale).

814 The NN employed to describe the potential energy surfaces in NNP-MD use as input
815 the Cartesian coordinates of each atom and provide, as output, the total energy and the
816 forces acting on each atom. These are calculated by considering the local environment of
817 each particle using either a local Cartesian frame of reference or a set of local descriptors
818 of the molecular configuration referred to as "symmetry functions" (first proposed by
819 Behler and Parrinello).[174, 175] The latter approach makes it easier to ensure permutational
820 symmetry of the energy function, i.e., the invariance of the latter upon exchange of labels
821 between identical particles. The total energy is then obtained through a summation over
822 the atoms atom as discussed in detail in Refs [174, 175]. While the NNP-MD implementation
823 by Behler and Parrinello requires prior definition of symmetry functions, the Deep
824 Potential techniques introduced by Weinan E's group can learn these on the fly and thus
825 requires only Cartesian coordinates as input.[176, 177] Multiple benchmarks indicate that
826 Deep Potential can reach AIMD accuracy at the computational cost not much higher than
827 classical simulations.[178]

828 There are several reports of NNP-MD simulations of water/oxide interfaces. One
829 example is the interfacial proton transfer at the water/ZnO($10\bar{1}0$) interface.[179] NNP-MD
830 simulations containing about 2000 atoms for nanosecond timescales were carried out and
831 proton transfer among surface OH groups and interfacial water were observed.[179] The
832 PMFs of proton transfer, based on the number of donated or accepted H-bonds, were
833 calculated and it was determined that water molecules that would lose a proton preferred
834 not to accept hydrogen bonds. However, due to the H-bond fluctuations, those water can
835 receive one more H-bond and the barrier of proton transfer decreases. Although the
836 fraction of interfacial water molecules accepting one H-bond is not the highest, it makes

the predominant contribution to proton transfer by what is called the "presolvation" mechanism. The simulation workload is much beyond what AIMD is able to handle and classical MD simulations are not able deal with proton transfer properly, demonstrating the power of NNP-MD simulation for investigating chemical reactions in complicated environments with AIMD-level accuracy and proper statistical significance. In later works, proton transfer at both water/ZnO $(10\bar{1}0)$ and $(11\bar{2}0)$ interfaces are also studied and different types of proton transfer are revealed.[180, 181] At the $(10\bar{1}0)$ surface, the proton diffusion coefficient along the $(1\bar{2}10)$ direction is about 20 times higher than that along the (0001) direction, indicating that proton transfer is "pseudo-one-dimensional"; however, at the $(11\bar{2}0)$ surface, proton transfer is two dimensional, along both the $(1\bar{1}00)$ and the (0001) directions (Figure 14). The NNP-MD simulations are also used to study the vibrational spectra of the water/ZnO$(10\bar{1}0)$ interface, finding that the frequency of water species within 4 Å of the surface will be perturbed from the bulk. They decompose the total OH vibrational spectra into contributions for each water species though their signals basically overlap together. This work shows that NNP-MD simulations can not only reproduce the structure and energy as AIMD, but it can also provide reliable dynamics. Now, NNP-MD has been implemented in LAMMPS.[182]

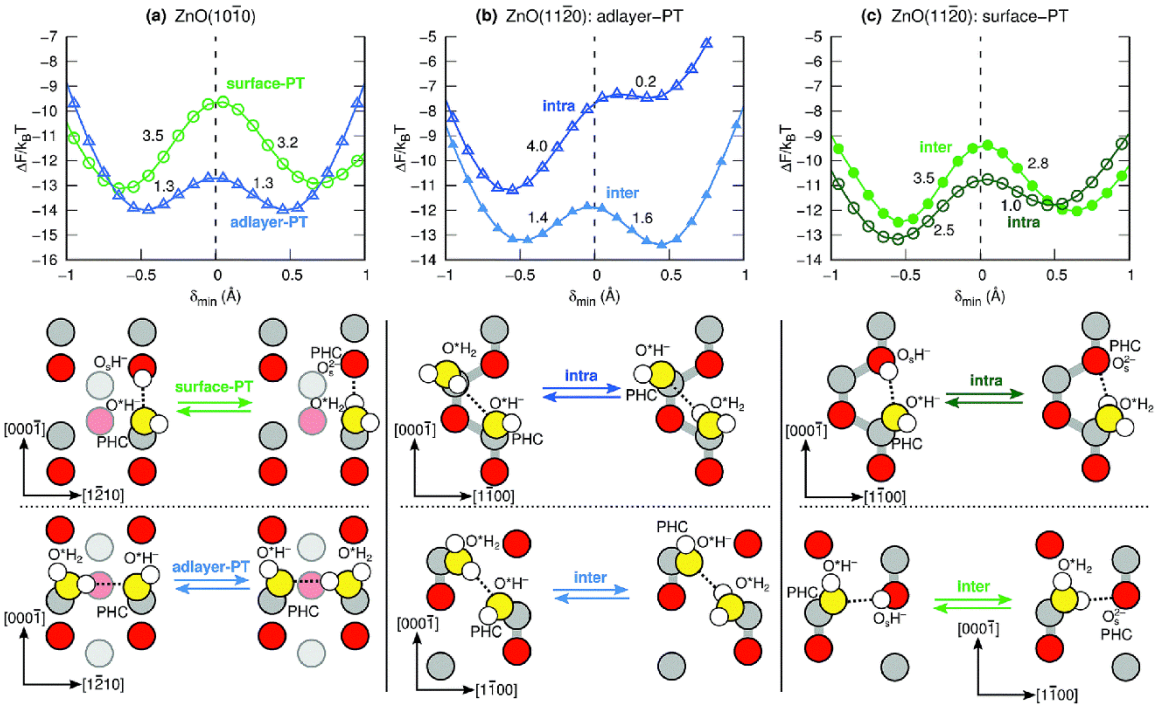

Figure 14. Free energy profile of proton transfer at the (a) ZnO(10$\bar{1}$0) interface and (b, c) ZnO (11$\bar{2}$0) interface. For the ZnO(10$\bar{1}$0) interface, proton transfer along the (0001) direction has a high barrier (3.5 k_BT, green in (a)), but that along the (1$\bar{2}$10) is more accessible. For the ZnO (11$\bar{2}$0) interface, proton transfer is along both two directions. Reprinted from Ref 180 - Published by The Royal Society of Chemistry.

The future and challenge of this field

As we pointed out in previous sections, applications of MD simulations have grown rapidly in recent years thanks to increased computational resources. However, MD simulations are not panaceas to investigate all chemical processes near water/oxide interfaces. We list several limitations and challenges of current MD simulations and expect that breakthroughs could be made to increase the impact of this field.

First, perfect, defect absent solid surfaces were used in most simulations as a model of "real" surfaces in experimental conditions. Such a simplification could be used for stable surfaces but in the real world, besides intrinsic defects of mineral crystals, dissolution and precipitation keep reshaping the interfaces. Howeever, how such processes affect local

water structure is unknown.

Second, when the ion concentration is low, the thickness of interfacial region could be as long as 10~100 nm, making simulations of the interfacial region at all-atomic level slow and ineffective. It will be a good practice to perform multiscale modeling with a simplified diffuse layer to reduce simulation cost and keep the interfacial region complete.

Some general limitations in MD simulations, such as the accuracy of force fields, limited time/length scales of simulations and neglect of nuclear quantum effects are not inevitable in simulations of water/oxide interfaces. Besides those theoretical concerns, we expect that more software tools could be developed to accelerate the preparation and analysis of simulation results, such as web-based CHARMM-GUI,[183] which supports modeling mineral surfaces. In addition, new technologies such as virtual reality could help the visualization of MD simulations.[184]

Summary

We have reviewed computational MD simulations of water/oxide interfaces, with a focus on chemical processes, such as water or small molecule adsorption, pKa calculation near interfaces and heterogeneous catalysis. The behavior of interfacial water is quite different from that in the bulk and more sophisticated descriptions than approximations based-on mean-field levels, such as EDL theory, are required. Solutes, such as ions or biomolecules, can adsorb onto the surface and further affect interfacial water structures. Using AIMD, the pKa of surface OH groups, the pKa of solutes near interfaces and how solutes affect surface pKa, can be investigated. From MD simulations, vibrational spectra, such as widely reported vSFG, can be calculated and compared with experimental measures. Chemical reactions at interfaces, such as catalytic water splitting at water/TiO_2 interfaces, can also be studied by MD simulations which reveal the estimated free energy profile and the catalytic mechanism. The microscopic insight provided by computational studies advances our understanding of the chemistry and physics at water/solid interfaces and complements experimental characterizations. Lastly, to overcome current limitations in classical MD and AIMD simulations, NNP-MD simulations can enlarge the scale of AIMD-like simulations to the level of classical simulations without the loss of accuracy at

a reasonable cost, which could be a promising method for MD simulations in the future.

Acknowledgements

This work was supported as part of the Center for Complex Materials from First Principles (CCM), an Energy Frontier Research Center funded by the U.S. Department of Energy, Office of Science, Basic Energy Sciences under Award #DE-SC0012575. This work was funded by the National Institutes of Health (R01GM093290, R01GM131048, S10OD020095 to V.C.), and the National Science Foundation grant IOS-1934848 to V.C.). R.W. thanks Temple University for the support of a Presidential Fellowship.

Corresponding Authors

*(E.B.) E-mail:eborguet@temple.edu.

*(V.C.) E-mail:vincenzo.carnevale@temple.edu.

Reference

1. Björneholm O, Hansen MH, Hodgson A, Liu L-M, Limmer DT, Michaelides A, et al. Water at Interfaces. Chem Rev. 2016;116(13):7698-726. DOI: 10.1021/acs.chemrev.6b00045

2. Taylor CD, Neurock M. Theoretical Insights into the Structure and Reactivity of the Aqueous/Metal Interface. Curr Opin Solid State Mater Sci. 2005;9(1):49-65. DOI: https://doi.org/10.1016/j.cossms.2006.03.007

3. Carrasco J, Hodgson A, Michaelides A. A Molecular Perspective of Water at Metal Interfaces. Nat Mater. 2012;11:667. DOI: 10.1038/nmat3354

4. Felix Sedlmeier JJ, Christian Sendner, Lyderic Bocquet, Roland R. Netz, and Dominik Horinek,. Water at Polar and Nonpolar Solid Walls (Review). Biointerphases. 2008;3(3):FC23-FC39. DOI: 10.1116/1.2999559

5. Rimola A, Sodupe M, Ugliengo P. Aluminosilicate Surfaces as Promoters for Peptide Bond Formation: An Assessment of Bernal's Hypothesis by Ab Initio Methods. J Am Chem Soc. 2007;129(26):8333-44. DOI: 10.1021/ja070451k

6. Rimola A, Sodupe M, Ugliengo P. Role of Mineral Surfaces in Prebiotic Chemical

933 Evolution. In Silico Quantum Mechanical Studies. Life. 2019;9(1):10. DOI:
934 10.3390/life9010010
935 7. Sakong S, Forster-Tonigold K, Groß A. The Structure of Water at a Pt(111) Electrode
936 and the Potential of Zero Charge Studied from First Principles. J Chem Phys.
937 2016;144(19):194701. DOI: 10.1063/1.4948638
938 8. McKendry IG, Thenuwara AC, Shumlas SL, Peng H, Aulin YV, Chinnam PR, et al.
939 Systematic Doping of Cobalt into Layered Manganese Oxide Sheets Substantially
940 Enhances Water Oxidation Catalysis. Inorg Chem. 2018;57(2):557-64. DOI:
941 10.1021/acs.inorgchem.7b01592
942 9. Attanayake NH, Thenuwara AC, Patra A, Aulin YV, Tran TM, Chakraborty H, et al.
943 Effect of Intercalated Metals on the Electrocatalytic Activity of 1T- MoS_2 for the Hydrogen
944 Evolution Reaction. ACS Energy Lett. 2018;3(1):7-13. DOI:
945 10.1021/acsenergylett.7b00865
946 10. Sakong S, Groß A. The Electric Double Layer at Metal-Water Interfaces Revisited
947 Based on a Charge Polarization Scheme. J Chem Phys. 2018;149(8). DOI:
948 10.1063/1.5040056
949 11. Helmholtz H. Studien Über Electrische Grenzschichten. Ann Phys. 1879;243(7):337-
950 82. DOI: 10.1002/andp.18792430702
951 12. Sposito G. Gouy-Chapman Theory. Encyclopedia of Geochemistry: A Comprehensive
952 Reference Source on the Chemistry of the Earth. Cham: Springer International Publishing;
953 2018. p. 623-8. DOI: 10.1007/978-3-319-39312-4_50
954 13. Chapman DL. Li. A Contribution to the Theory of Electrocapillarity. The London,
955 Edinburgh, and Dublin Philosophical Magazine and Journal of Science. 1913;25(148):475-
956 81. DOI: 10.1080/14786440408634187
957 14. Gouy M. Sur La Constitution De La Charge Électrique À La Surface D'un Électrolyte.
958 J Phys Theor Appl. 1910;9(1):457-68. DOI: 10.1051/jphystap:019100090045700
959 15. Backus E, Schaefer J, Bonn M. The Mineral/Water Interface Probed with Nonlinear
960 Optical Spectroscopy. Angew Chem Int Ed. 2020. DOI: 10.1002/anie.202003085
961 16. Stern O. Zur Theorie Der Elektrolytischen Doppelschicht. Zeitschrift für
962 Elektrochemie und angewandte physikalische Chemie. 1924;30(21-22):508-16. DOI:

963 10.1002/bbpc.192400182
964 17. Elimelech M, Gregory J, Jia X, Williams RA. Chapter 2 - Electrical Properties of
965 Interfaces. Particle Deposition & Aggregation. Woburn: Butterworth-Heinemann; 1995.
966 p. 9-32. DOI: https://doi.org/10.1016/B978-075067024-1/50002-9
967 18. Dewan S, Carnevale V, Bankura A, Eftekhari-Bafrooei A, Fiorin G, Klein ML, et al.
968 Structure of Water at Charged Interfaces: A Molecular Dynamics Study. Langmuir.
969 2014;30(27):8056-65. DOI: 10.1021/la5011055
970 19. Fenter P, Sturchio NC. Mineral–Water Interfacial Structures Revealed by Synchrotron
971 X-Ray Scattering. Prog Surf Sci. 2004;77(5):171-258. DOI:
972 https://doi.org/10.1016/j.progsurf.2004.12.001
973 20. Santos S, Verdaguer A. Imaging Water Thin Films in Ambient Conditions Using
974 Atomic Force Microscopy. Materials. 2016;9(3):182. DOI: 10.3390/ma9030182
975 21. Mu R, Zhao Z-j, Dohnálek Z, Gong J. Structural Motifs of Water on Metal Oxide
976 Surfaces. Chem Soc Rev. 2017;46(7):1785-806. DOI: 10.1039/C6CS00864J
977 22. Covert PA, Hore DK. Geochemical Insight from Nonlinear Optical Studies of
978 Mineral–Water Interfaces. Annu Rev Phys Chem. 2016;67(1):233-57. DOI:
979 10.1146/annurev-physchem-040215-112300
980 23. Takagi Y, Uruga T, Tada M, Iwasawa Y, Yokoyama T. Ambient Pressure Hard X-Ray
981 Photoelectron Spectroscopy for Functional Material Systems as Fuel Cells under Working
982 Conditions. Acc Chem Res. 2018;51(3):719-27. DOI: 10.1021/acs.accounts.7b00563
983 24. Cyran JD, Donovan MA, Vollmer D, Siro Brigiano F, Pezzotti S, Galimberti DR, et al.
984 Molecular Hydrophobicity at a Macroscopically Hydrophilic Surface. Proc Natl Acad Sci
985 U S A. 2019;116(5):1520-5. DOI: 10.1073/pnas.1819000116
986 25. Lamour G, Hamraoui A, Buvailo A, Xing Y, Keuleyan S, Prakash V, et al. Contact
987 Angle Measurements Using a Simplified Experimental Setup. J Chem Educ.
988 2010;87(12):1403-7. DOI: 10.1021/ed100468u
989 26. Harmon KJ, Chen Y, Bylaska EJ, Catalano JG, Bedzyk MJ, Weare JH, et al. Insights
990 on the Alumina–Water Interface Structure by Direct Comparison of Density Functional
991 Simulations with X-Ray Reflectivity. J Phys Chem C. 2018;122(47):26934-44. DOI:
992 10.1021/acs.jpcc.8b08522

27. Catalano JG. Weak Interfacial Water Ordering on Isostructural Hematite and Corundum (0 0 1) Surfaces. Geochim Cosmochim Acta. 2011;75(8):2062-71. DOI: http://dx.doi.org/10.1016/j.gca.2011.01.025

28. Catalano JG. Relaxations and Interfacial Water Ordering at the Corundum (110) Surface. J Phys Chem C. 2010;114(14):6624-30. DOI: 10.1021/jp100455s

29. Catalano JG, Park C, Zhang Z, Fenter P. Termination and Water Adsorption at the α-Al_2O_3(012)−Aqueous Solution Interface. Langmuir. 2006;22(10):4668-73. DOI: 10.1021/la060177s

30. Tuladhar A, Piontek SM, Frazer L, Borguet E. Effect of Halide Anions on the Structure and Dynamics of Water Next to an Alumina (0001) Surface. J Phys Chem C. 2018;122(24):12819-30. DOI: 10.1021/acs.jpcc.8b03004

31. Tuladhar A, Piontek SM, Borguet E. Insights on Interfacial Structure, Dynamics, and Proton Transfer from Ultrafast Vibrational Sum Frequency Generation Spectroscopy of the Alumina(0001)/Water Interface. J Phys Chem C. 2017;121(9):5168-77. DOI: 10.1021/acs.jpcc.7b00499

32. Tuladhar A, Dewan S, Kubicki JD, Borguet E. Spectroscopy and Ultrafast Vibrational Dynamics of Strongly Hydrogen Bonded OH Species at the α-Al_2O_3 ($11\bar{2}0$)/H_2O Interface. J Phys Chem C. 2016;120(29):16153-61. DOI: 10.1021/acs.jpcc.5b12486

33. Humphrey W, Dalke A, Schulten K. VMD: Visual Molecular Dynamics. J Mol Graph. 1996;14(1):33-8. DOI: http://dx.doi.org/10.1016/0263-7855(96)00018-5

34. McGibbon RT, Beauchamp KA, Harrigan MP, Klein C, Swails JM, Hernández CX, et al. MDTraj: A Modern Open Library for the Analysis of Molecular Dynamics Trajectories. Biophys J. 2015;109(8):1528-32. DOI: 10.1016/j.bpj.2015.08.015

35. Richard J. Gowers ML, Jonathan Barnoud, Tyler J. E. Reddy, Manuel N. Melo, Sean L. Seyler, Jan Domański, David L. Dotson, Sébastien Buchoux, Ian M. Kenney and Oliver Beckstein. MDAnalysis: A Python Package for the Rapid Analysis of Molecular Dynamics Simulations. Proceedings of the 15th Python in Science Conference2016. p. 98 - 105. DOI: 10.25080/Majora-629e541a-00e

36. Michaud-Agrawal N, Denning EJ, Woolf TB, Beckstein O. MDAnalysis: A Toolkit for the Analysis of Molecular Dynamics Simulations. J Comput Chem. 2011;32(10):2319-27.

DOI: 10.1002/jcc.21787
37. Striolo A. From Interfacial Water to Macroscopic Observables: A Review. Adsorpt Sci Technol. 2011;29(3):211-58. DOI: 10.1260/0263-6174.29.3.211
38. Striolo A, Michaelides A, Joly L. The Carbon-Water Interface: Modeling Challenges and Opportunities for the Water-Energy Nexus. Annu Rev Chem Biomol Eng. 2016;7(1):533-56. DOI: 10.1146/annurev-chembioeng-080615-034455
39. YazdanYar A, Aschauer U, Bowen P. Interaction of Biologically Relevant Ions and Organic Molecules with Titanium Oxide (Rutile) Surfaces: A Review on Molecular Dynamics Studies. Colloids Surf B Biointerfaces. 2018;161:563-77. DOI: https://doi.org/10.1016/j.colsurfb.2017.11.004
40. Verlet L. Computer "Experiments" on Classical Fluids. I. Thermodynamical Properties of Lennard-Jones Molecules. Phys Rev. 1967;159(1):98-103. DOI: 10.1103/PhysRev.159.98
41. Frenkel D, Smit B. Understanding Molecular Simulation: From Algorithms to Applications: Elsevier; 2001. DOI: https://doi.org/10.1016/B978-0-12-267351-1.X5000-7
42. Allen MP, Tildesley DJ. Computer Simulation of Liquids: Oxford university press; 2017.
43. Phillips JC, Braun R, Wang W, Gumbart J, Tajkhorshid E, Villa E, et al. Scalable Molecular Dynamics with NAMD. J Comput Chem. 2005;26(16):1781-802. DOI: 10.1002/jcc.20289
44. Demerdash O, Wang LP, Head-Gordon T. Advanced Models for Water Simulations. WIREs Comput Mol Sci. 2018;8(1):e1355. DOI: doi:10.1002/wcms.1355
45. Remsing RC, Duignan TT, Baer MD, Schenter GK, Mundy CJ, Weeks JD. Water Lone Pair Delocalization in Classical and Quantum Descriptions of the Hydration of Model Ions. J Phys Chem B. 2018;122(13):3519-27. DOI: 10.1021/acs.jpcb.7b10722
46. van Duin ACT, Dasgupta S, Lorant F, Goddard WA. Reaxff: A Reactive Force Field for Hydrocarbons. J Phys Chem A. 2001;105(41):9396-409. DOI: 10.1021/jp004368u
47. Baskes MI. Modified Embedded-Atom Potentials for Cubic Materials and Impurities. Phys Rev B. 1992;46(5):2727-42. DOI: 10.1103/PhysRevB.46.2727
48. Shan T-R, Devine BD, Kemper TW, Sinnott SB, Phillpot SR. Charge-Optimized

Many-Body Potential for the Hafnium/Hafnium Oxide System. Phys Rev B. 2010;81(12):125328. DOI: 10.1103/PhysRevB.81.125328
49. Raju M, Kim S-Y, van Duin ACT, Fichthorn KA. ReaxFF Reactive Force Field Study of the Dissociation of Water on Titania Surfaces. J Phys Chem C. 2013;117(20):10558-72. DOI: 10.1021/jp402139h
50. Senftle TP, Hong S, Islam MM, Kylasa SB, Zheng Y, Shin YK, et al. The ReaxFF Reactive Force-Field: Development, Applications and Future Directions. Npj Computational Materials. 2016;2:15011. DOI: 10.1038/npjcompumats.2015.11
51. Car R, Parrinello M. Unified Approach for Molecular Dynamics and Density-Functional Theory. Phys Rev Lett. 1985;55(22):2471-4. DOI: 10.1103/PhysRevLett.55.2471
52. Iftimie R, Minary P, Tuckerman ME. Ab Initio Molecular Dynamics: Concepts, Recent Developments, and Future Trends. Proc Natl Acad Sci U S A. 2005;102(19):6654-9. DOI: 10.1073/pnas.0500193102
53. Alder BJ, Wainwright TE. Phase Transition for a Hard Sphere System. J Chem Phys. 1957;27(5):1208-9. DOI: 10.1063/1.1743957
54. Rahman A. Correlations in the Motion of Atoms in Liquid Argon. Phys Rev. 1964;136(2A):A405-A11. DOI: 10.1103/PhysRev.136.A405
55. Rahman A, Stillinger FH. Molecular Dynamics Study of Liquid Water. J Chem Phys. 1971;55(7):3336-59. DOI: 10.1063/1.1676585
56. Watanabe H, Suzuki M, Ito N. Huge-Scale Molecular Dynamics Simulation of Multibubble Nuclei. Comput Phys Commun. 2013;184(12):2775-84. DOI: https://doi.org/10.1016/j.cpc.2013.07.023
57. Shaw DE, Dror RO, Salmon JK, Grossman J, Mackenzie KM, Bank JA, et al. Millisecond-Scale Molecular Dynamics Simulations on Anton. Proceedings of the conference on high performance computing networking, storage and analysis; 2009.
58. Baer MD, Kuo IFW, Tobias DJ, Mundy CJ. Toward a Unified Picture of the Water Self-Ions at the Air–Water Interface: A Density Functional Theory Perspective. J Phys Chem B. 2014;118(28):8364-72. DOI: 10.1021/jp501854h
59. Cheng J, Liu X, VandeVondele J, Sprik M. Reductive Hydrogenation of the Aqueous

Rutile TiO_2(110) Surface. Electrochim Acta. 2015;179:658-67. DOI: https://doi.org/10.1016/j.electacta.2015.03.212

60. Hass KC, Schneider WF, Curioni A, Andreoni W. The Chemistry of Water on Alumina Surfaces: Reaction Dynamics from First Principles. Science. 1998;282(5387):265-8. DOI: 10.1126/science.282.5387.265

61. Hass KC, Schneider WF, Curioni A, Andreoni W. First-Principles Molecular Dynamics Simulations of H_2O on α-Al_2O_3 (0001). J Phys Chem B. 2000;104(23):5527-40. DOI: 10.1021/jp000040p

62. Hoover WG. Canonical Dynamics: Equilibrium Phase-Space Distributions. Phys Rev A. 1985;31(3):1695-7. DOI: 10.1103/PhysRevA.31.1695

63. Nosé S. A Unified Formulation of the Constant Temperature Molecular Dynamics Methods. J Chem Phys. 1984;81(1):511-9. DOI: 10.1063/1.447334

64. Nosé S. A Molecular Dynamics Method for Simulations in the Canonical Ensemble. Mol Phys. 1984;52(2):255-68. DOI: 10.1080/00268978400101201

65. Martyna GJ, Tuckerman ME, Tobias DJ, Klein ML. Explicit Reversible Integrators for Extended Systems Dynamics. Mol Phys. 1996;87(5):1117-57. DOI: 10.1080/00268979600100761

66. Rimola A, Costa D, Sodupe M, Lambert JF, Ugliengo P. Silica Surface Features and Their Role in the Adsorption of Biomolecules: Computational Modeling and Experiments. Chem Rev. 2013;113(6):4216-313. DOI: 10.1021/cr3003054

67. Frank ES, Fan H, Shrestha M, Riahi S, Tobias DJ, Grassian VH. Impact of Adsorbed Water on the Interaction of Limonene with Hydroxylated SiO_2: Implications of π-Hydrogen Bonding for Surfaces in Humid Environments. J Phys Chem A. 2020;124(50):10592-9. DOI: 10.1021/acs.jpca.0c08600

68. Jia J, Liang Y, Tsuji T, Miranda CR, Masuda Y, Matsuoka T. Ab Initio Molecular Dynamics Study of Carbonation and Hydrolysis Reactions on Cleaved Quartz (001) Surface. J Phys Chem C. 2019;123(8):4938-48. DOI: 10.1021/acs.jpcc.8b12089

69. Rimola A, Fabbiani M, Sodupe M, Ugliengo P, Martra G. How Does Silica Catalyze the Amide Bond Formation under Dry Conditions? Role of Specific Surface Silanol Pairs. ACS Catal. 2018;8(5):4558-68. DOI: 10.1021/acscatal.7b03961

70. Anderson RS, Anderson SP. Geomorphology: The Mechanics and Chemistry of Landscapes. Cambridge: Cambridge University Press; 2010. DOI: 10.1017/CBO9780511794827

71. Ong S, Zhao X, Eisenthal KB. Polarization of Water Molecules at a Charged Interface: Second Harmonic Studies of the Silica/Water Interface. Chem Phys Lett. 1992;191(3):327-35. DOI: https://doi.org/10.1016/0009-2614(92)85309-X

72. Gaigeot M-P, Sprik M, Sulpizi M. Oxide/Water Interfaces: How the Surface Chemistry Modifies Interfacial Water Properties. J Phys: Condens Matter. 2012;24(12):124106. DOI: 10.1088/0953-8984/24/12/124106

73. Hocine S, Hartkamp R, Siboulet B, Duvail M, Coasne B, Turq P, et al. How Ion Condensation Occurs at a Charged Surface: A Molecular Dynamics Investigation of the Stern Layer for Water–Silica Interfaces. J Phys Chem C. 2016;120(2):963-73. DOI: 10.1021/acs.jpcc.5b08836

74. Bouhadja M, Skelton AA. Dynamical Properties of Water and Ions at the Quartz (101)–Water Interface at a Range of Solution Conditions: A Classical Molecular Dynamics Study. J Phys Chem C. 2018;122(3):1535-46. DOI: 10.1021/acs.jpcc.7b08214

75. Kroutil O, Chval Z, Skelton AA, Předota M. Computer Simulations of Quartz (101)–Water Interface over a Range of pH Values. J Phys Chem C. 2015;119(17):9274-86. DOI: 10.1021/acs.jpcc.5b00096

76. Brkljača Z, Namjesnik D, Lützenkirchen J, Předota M, Preočanin T. Quartz/Aqueous Electrolyte Solution Interface: Molecular Dynamic Simulation and Interfacial Potential Measurements. J Phys Chem C. 2018;122(42):24025-36. DOI: 10.1021/acs.jpcc.8b04035

77. Quezada GR, Rozas RE, Toledo PG. Molecular Dynamics Simulations of Quartz (101)–Water and Corundum (001)–Water Interfaces: Effect of Surface Charge and Ions on Cation Adsorption, Water Orientation, and Surface Charge Reversal. J Phys Chem C. 2017;121(45):25271-82. DOI: 10.1021/acs.jpcc.7b08836

78. Pfeiffer-Laplaud M, Gaigeot MP. Adsorption of Singly Charged Ions at the Hydroxylated (0001) α-Quartz/Water Interface. J Phys Chem C. 2016;120(9):4866-80. DOI: 10.1021/acs.jpcc.5b10947

79. DelloStritto MJ, Kubicki JD, Sofo JO. Effect of Ions on H-Bond Structure and

Dynamics at the Quartz(101)–Water Interface. Langmuir. 2016;32(44):11353-65. DOI: 10.1021/acs.langmuir.6b01719
80. Leung K, Criscenti LJ, Knight AW, Ilgen AG, Ho TA, Greathouse JA. Concerted Metal Cation Desorption and Proton Transfer on Deprotonated Silica Surfaces. J Phys Chem Lett. 2018;9(18):5379-85. DOI: 10.1021/acs.jpclett.8b02173
81. Pfeiffer-Laplaud M, Gaigeot MP. Electrolytes at the Hydroxylated (0001) α-Quartz/Water Interface: Location and Structural Effects on Interfacial Silanols by DFT-Based Md. J Phys Chem C. 2016;120(26):14034-47. DOI: 10.1021/acs.jpcc.6b01819
82. Chen S-H, Singer SJ. Molecular Dynamics Study of the Electric Double Layer and Nonlinear Spectroscopy at the Amorphous Silica–Water Interface. J Phys Chem B. 2019;123(29):6364-84. DOI: 10.1021/acs.jpcb.9b05871
83. Kolman K, Abbas Z. Molecular Dynamics Exploration for the Adsorption of Benzoic Acid Derivatives on Charged Silica Surfaces. Colloids Surf Physicochem Eng Aspects. 2019;578:123635. DOI: https://doi.org/10.1016/j.colsurfa.2019.123635
84. Döpke MF, Lützenkirchen J, Moultos OA, Siboulet B, Dufrêche J-F, Padding JT, et al. Preferential Adsorption in Mixed Electrolytes Confined by Charged Amorphous Silica. J Phys Chem C. 2019;123(27):16711-20. DOI: 10.1021/acs.jpcc.9b02975
85. Buch V, Milet A, Vácha R, Jungwirth P, Devlin JP. Water Surface is Acidic. Proc Natl Acad Sci U S A. 2007;104(18):7342-7. DOI: 10.1073/pnas.0611285104
86. Tse Y-LS, Chen C, Lindberg GE, Kumar R, Voth GA. Propensity of Hydrated Excess Protons and Hydroxide Anions for the Air–Water Interface. J Am Chem Soc. 2015;137(39):12610-6. DOI: 10.1021/jacs.5b07232
87. Pezzotti S, Gaigeot M-P. Spectroscopic BIL-SFG Invariance Hides the Chaotropic Effect of Protons at the Air-Water Interface. Atmosphere. 2018;9(10):396. DOI: 10.3390/atmos9100396
88. Giberti F, Hassanali AA. The Excess Proton at the Air-Water Interface: The Role of Instantaneous Liquid Interfaces. J Chem Phys. 2017;146(24):244703. DOI: 10.1063/1.4986082
89. Mundy CJ, Kuo IFW, Tuckerman ME, Lee H-S, Tobias DJ. Hydroxide Anion at the Air–Water Interface. Chem Phys Lett. 2009;481(1):2-8. DOI:

https://doi.org/10.1016/j.cplett.2009.09.003
90. Beattie JK, Djerdjev AM, Warr GG. The Surface of Neat Water is Basic. Faraday Discuss. 2009;141(0):31-9. DOI: 10.1039/B805266B
91. Mishra H, Enami S, Nielsen RJ, Stewart LA, Hoffmann MR, Goddard WA, et al. Brønsted Basicity of the Air–Water Interface. Proc Natl Acad Sci U S A. 2012:201209307. DOI: 10.1073/pnas.1209307109
92. Sulpizi M, Gaigeot M-P, Sprik M. The Silica–Water Interface: How the Silanols Determine the Surface Acidity and Modulate the Water Properties. J Chem Theory Comput. 2012;8(3):1037-47. DOI: 10.1021/ct2007154
93. Pfeiffer-Laplaud M, Gaigeot MP, Sulpizi M. pK_a at Quartz/Electrolyte Interfaces. J Phys Chem Lett. 2016;7(16):3229-34. DOI: 10.1021/acs.jpclett.6b01422
94. Pfeiffer-Laplaud M, Costa D, Tielens F, Gaigeot MP, Sulpizi M. Bimodal Acidity at the Amorphous Silica/Water Interface. J Phys Chem C. 2015;119(49):27354-62. DOI: 10.1021/acs.jpcc.5b02854
95. Parashar S, Lesnicki D, Sulpizi M. Increased Acid Dissociation at the Quartz/Water Interface. J Phys Chem Lett. 2018;9(9):2186-9. DOI: 10.1021/acs.jpclett.8b00686
96. Sulpizi M, Sprik M. Acidity Constants from Vertical Energy Gaps: Density Functional Theory Based Molecular Dynamics Implementation. Phys Chem Chem Phys. 2008;10(34):5238-49. DOI: 10.1039/B802376J
97. Joutsuka T, Hirano T, Sprik M, Morita A. Effects of Third-Order Susceptibility in Sum Frequency Generation Spectra: A Molecular Dynamics Study in Liquid Water. Phys Chem Chem Phys. 2018;20(5):3040-53. DOI: 10.1039/C7CP01978E
98. Morita A, Ishiyama T. Recent Progress in Theoretical Analysis of Vibrational Sum Frequency Generation Spectroscopy. Phys Chem Chem Phys. 2008;10(38):5801-16. DOI: 10.1039/B808110G
99. Pezzotti S, Galimberti DR, Shen YR, Gaigeot M-P. Structural Definition of the BIL and DL: A New Universal Methodology to Rationalize Non-Linear $\chi^{(2)}(\omega)$ SFG Signals at Charged Interfaces, Including $\chi^{(3)}(\omega)$ Contributions. Phys Chem Chem Phys. 2018;20(7):5190-9. DOI: 10.1039/C7CP06110B
100. Pezzotti S, Galimberti DR, Gaigeot M-P. Deconvolution of BIL-SFG and DL-SFG

1203 Spectroscopic Signals Reveals Order/Disorder of Water at the Elusive Aqueous Silica
1204 Interface. Phys Chem Chem Phys. 2019;21(40):22188-202. DOI: 10.1039/C9CP02766A
1205 101. Ohto T, Dodia M, Xu J, Imoto S, Tang F, Zysk F, et al. Accessing the Accuracy of
1206 Density Functional Theory through Structure and Dynamics of the Water–Air Interface. J
1207 Phys Chem Lett. 2019;10(17):4914-9. DOI: 10.1021/acs.jpclett.9b01983
1208 102. Smit WJ, Tang F, Sánchez MA, Backus EHG, Xu L, Hasegawa T, et al. Excess
1209 Hydrogen Bond at the Ice-Vapor Interface around 200 K. Phys Rev Lett.
1210 2017;119(13):133003. DOI: 10.1103/PhysRevLett.119.133003
1211 103. Reddy SK, Thiraux R, Wellen Rudd BA, Lin L, Adel T, Joutsuka T, et al. Bulk
1212 Contributions Modulate the Sum-Frequency Generation Spectra of Water on Model Sea-
1213 Spray Aerosols. Chem. 2018;4(7):1629-44. DOI:
1214 https://doi.org/10.1016/j.chempr.2018.04.007
1215 104. Seki T, Sun S, Zhong K, Yu C-C, Machel K, Dreier LB, et al. Unveiling
1216 Heterogeneity of Interfacial Water through the Water Bending Mode. J Phys Chem Lett.
1217 2019;10(21):6936-41. DOI: 10.1021/acs.jpclett.9b02748
1218 105. Wen Y-C, Zha S, Liu X, Yang S, Guo P, Shi G, et al. Unveiling Microscopic
1219 Structures of Charged Water Interfaces by Surface-Specific Vibrational Spectroscopy. Phys
1220 Rev Lett. 2016;116(1):016101
1221 106. Fertani-Gmati M, Jemal M. Thermochemistry and Kinetics of Silica Dissolution
1222 in Naoh Aqueous Solution. Thermochim Acta. 2011;513(1):43-8. DOI:
1223 https://doi.org/10.1016/j.tca.2010.11.008
1224 107. Du J, Rimsza JM. Atomistic Computer Simulations of Water Interactions and
1225 Dissolution of Inorganic Glasses. npj Materials Degradation. 2017;1(1):16. DOI:
1226 10.1038/s41529-017-0017-y
1227 108. Rimsza JM, Yeon J, van Duin ACT, Du J. Water Interactions with Nanoporous
1228 Silica: Comparison of ReaxFF and Ab Initio Based Molecular Dynamics Simulations. J
1229 Phys Chem C. 2016;120(43):24803-16. DOI: 10.1021/acs.jpcc.6b07939
1230 109. Rimsza JM, Du J. Interfacial Structure and Evolution of the Water–Silica Gel
1231 System by Reactive Force-Field-Based Molecular Dynamics Simulations. J Phys Chem C.
1232 2017;121(21):11534-43. DOI: 10.1021/acs.jpcc.7b02734

110. Santos PS, Santos HS, Toledo SP. Standard Transition Aluminas. Electron Microscopy Studies. Materials Research. 2000;3:104-14. DOI: 10.1590/S1516-14392000000400003
111. Feng JT, He YF, Liu YN, Du YY, Li DQ. Supported Catalysts Based on Layered Double Hydroxides for Catalytic Oxidation and Hydrogenation: General Functionality and Promising Application Prospects. Chem Soc Rev. 2015;44(15):5291-319. DOI: 10.1039/c5cs00268k
112. Réocreux R, Jiang T, Iannuzzi M, Michel C, Sautet P. Structuration and Dynamics of Interfacial Liquid Water at Hydrated γ-Alumina Determined by Ab Initio Molecular Simulations: Implications for Nanoparticle Stability. ACS Appl Nano Mater. 2018;1(1):191-9. DOI: 10.1021/acsanm.7b00100
113. Argyris D, Ho T, Cole DR, Striolo A. Molecular Dynamics Studies of Interfacial Water at the Alumina Surface. J Phys Chem C. 2011;115(5):2038-46. DOI: 10.1021/jp109244c
114. Ridley MK, Tunega D. Insights on the Structural and Dynamic Properties of Corundum–Water Interfaces from First-Principle Molecular Dynamics. J Phys Chem C. 2020. DOI: 10.1021/acs.jpcc.0c06554
115. Wang R, DelloStritto M, Remsing RC, Carnevale V, Klein ML, Borguet E. Sodium Halide Adsorption and Water Structure at the α-Alumina(0001)/Water Interface. J Phys Chem C. 2019;123(25):15618-28. DOI: 10.1021/acs.jpcc.9b03054
116. Cygan RT, Liang J-J, Kalinichev AG. Molecular Models of Hydroxide, Oxyhydroxide, and Clay Phases and the Development of a General Force Field. J Phys Chem B. 2004;108(4):1255-66. DOI: 10.1021/jp0363287
117. Pouvreau M, Greathouse JA, Cygan RT, Kalinichev AG. Structure of Hydrated Kaolinite Edge Surfaces: DFT Results and Further Development of the ClayFF Classical Force Field with Metal–O–H Angle Bending Terms. J Phys Chem C. 2019;123(18):11628-38. DOI: 10.1021/acs.jpcc.9b00514
118. DelloStritto M, Sofo J. Bond Polarizability Model for Sum Frequency Generation at the Al_2O_3(0001)–H_2O Interface. J Phys Chem A. 2017;121(16):3045-55. DOI: 10.1021/acs.jpca.7b00862
119. Braunschweig B, Eissner S, Daum W. Molecular Structure of a Mineral/Water Interface: Effects of Surface Nanoroughness of α-Al_2O_3(0001). J Phys Chem C.

2008;112(6):1751-4. DOI: 10.1021/jp711758y

120. DelloStritto M, Piontek SM, Klein ML, Borguet E. Relating Interfacial Order to Sum Frequency Generation with Ab Initio Simulations of the Aqueous Al_2O_3(0001) and ($11\bar{2}0$) Interfaces. J Phys Chem C. 2018;122(37):21284-94. DOI: 10.1021/acs.jpcc.8b02809

121. DelloStritto MJ, Piontek SM, Klein ML, Borguet E. Effect of Functional and Electron Correlation on the Structure and Spectroscopy of the Al_2O_3(001)–H_2O Interface. J Phys Chem Lett. 2019;10(9):2031-6. DOI: 10.1021/acs.jpclett.9b00016

122. Sun J, Ruzsinszky A, Perdew JP. Strongly Constrained and Appropriately Normed Semilocal Density Functional. Phys Rev Lett. 2015;115(3):036402. DOI: 10.1103/PhysRevLett.115.036402

123. Chen M, Ko H-Y, Remsing RC, Calegari Andrade MF, Santra B, Sun Z, et al. Ab Initio Theory and Modeling of Water. Proc Natl Acad Sci U S A. 2017:201712499. DOI: 10.1073/pnas.1712499114

124. Zheng L, Chen M, Sun Z, Ko H-Y, Santra B, Dhuvad P, et al. Structural, Electronic, and Dynamical Properties of Liquid Water by Ab Initio Molecular Dynamics Based on SCAN Functional within the Canonical Ensemble. J Chem Phys. 2018;148(16):164505. DOI: 10.1063/1.5023611

125. Xu J, Chen M, Zhang C, Wu X. First-Principles Study of the Infrared Spectrum in Liquid Water from a Systematically Improved Description of H-Bond Network. Phys Rev B. 2019;99(20):205123. DOI: 10.1103/PhysRevB.99.205123

126. Wang R, Carnevale V, Klein ML, Borguet E. First-Principles Calculation of Water pK_a Using the Newly Developed SCAN Functional. J Phys Chem Lett. 2020;11:54-9. DOI: 10.1021/acs.jpclett.9b02913

127. DelloStritto M, Xu J, Wu X, Klein ML. Aqueous Solvation of the Chloride Ion Revisited with Density Functional Theory: Impact of Correlation and Exchange Approximations. Phys Chem Chem Phys. 2020;22(19):10666-75. DOI: 10.1039/C9CP06821J

128. Melani G, Nagata Y, Wirth J, Saalfrank P. Vibrational Spectroscopy of Hydroxylated α-Al_2O_3(0001) Surfaces with and without Water: An Ab Initio Molecular

Dynamics Study. J Chem Phys. 2018;149(1):014707. DOI: 10.1063/1.5023347
129. Harmon KJ, Letchworth-Weaver K, Gaiduk AP, Giberti F, Gygi F, Chan MKY, et al. Validating First-Principles Molecular Dynamics Calculations of Oxide/Water Interfaces with X-Ray Reflectivity Data. Phys Rev Mater. 2020;4(11):113805. DOI: 10.1103/PhysRevMaterials.4.113805
130. Liu X, Cheng J, Sprik M, Lu X, Wang R. Understanding Surface Acidity of Gibbsite with First Principles Molecular Dynamics Simulations. Geochim Cosmochim Acta. 2013;120:487-95. DOI: https://doi.org/10.1016/j.gca.2013.06.043
131. Contescu C, Jagiello J, Schwarz JA. Heterogeneity of Proton Binding Sites at the Oxide/Solution Interface. Langmuir. 1993;9(7):1754-65. DOI: 10.1021/la00031a024
132. Gittus OR, von Rudorff GF, Rosso KM, Blumberger J. Acidity Constants of the Hematite–Liquid Water Interface from Ab Initio Molecular Dynamics. J Phys Chem Lett. 2018;9(18):5574-82. DOI: 10.1021/acs.jpclett.8b01870
133. Jia M, Zhang C, Cox SJ, Sprik M, Cheng J. Computing Surface Acidity Constants of Proton Hopping Groups from Density Functional Theory-Based Molecular Dynamics: Application to the SnO_2(110)/H_2O Interface. J Chem Theory Comput. 2020;16(10):6520-7. DOI: 10.1021/acs.jctc.0c00021
134. Diebold U. The Surface Science of Titanium Dioxide. Surf Sci Rep. 2003;48(5):53-229. DOI: https://doi.org/10.1016/S0167-5729(02)00100-0
135. Sun C, Liu L-M, Selloni A, Lu GQ, Smith SC. Titania-Water Interactions: A Review of Theoretical Studies. J Mater Chem. 2010;20(46):10319-34. DOI: 10.1039/C0JM01491E
136. Selcuk S, Selloni A. Excess Electrons at Anatase TiO_2 Surfaces and Interfaces: Insights from First Principles Simulations. J Phys D: Appl Phys. 2017;50(27). DOI: 10.1088/1361-6463/aa7540
137. Bourikas K, Kordulis C, Lycourghiotis A. Titanium Dioxide (Anatase and Rutile): Surface Chemistry, Liquid–Solid Interface Chemistry, and Scientific Synthesis of Supported Catalysts. Chem Rev. 2014;114(19):9754-823. DOI: 10.1021/cr300230q
138. Hosseinpour S, Tang F, Wang F, Livingstone RA, Schlegel SJ, Ohto T, et al. Chemisorbed and Physisorbed Water at the TiO_2/Water Interface. J Phys Chem Lett.

2017;8(10):2195-9. DOI: 10.1021/acs.jpclett.7b00564
139. Calegari Andrade MF, Ko H-Y, Car R, Selloni A. Structure, Polarization, and Sum Frequency Generation Spectrum of Interfacial Water on Anatase TiO_2. J Phys Chem Lett. 2018;9(23):6716-21. DOI: 10.1021/acs.jpclett.8b03103
140. Futera Z, English NJ. Exploring Rutile (110) and Anatase (101) TiO_2 Water Interfaces by Reactive Force-Field Simulations. J Phys Chem C. 2017;121(12):6701-11. DOI: 10.1021/acs.jpcc.6b12803
141. Holmström E, Ghan S, Asakawa H, Fujita Y, Fukuma T, Kamimura S, et al. Hydration Structure of Brookite TiO_2(210). J Phys Chem C. 2017;121(38):20790-801. DOI: 10.1021/acs.jpcc.7b05524
142. Zheng Z, Huang B, Lu J, Wang Z, Qin X, Zhang X, et al. Hydrogenated Titania: Synergy of Surface Modification and Morphology Improvement for Enhanced Photocatalytic Activity. Chem Commun. 2012;48(46):5733-5. DOI: 10.1039/C2CC32220J
143. Tan T, Xie J, Wang W, Ping H, Ma P, Xie H, et al. A Bio-Inspired Strategy for Enhanced Hydrogen Evolution: Carbonate Ions as Hole Vehicles to Promote Carrier Separation. Nanoscale. 2019;11(24):11451-6. DOI: 10.1039/C9NR04057A
144. Fujishima A, Honda K. Electrochemical Photolysis of Water at a Semiconductor Electrode. Nature. 1972;238(5358):37-8. DOI: 10.1038/238037a0
145. Li Y-F, Liu Z-P, Liu L, Gao W. Mechanism and Activity of Photocatalytic Oxygen Evolution on Titania Anatase in Aqueous Surroundings. J Am Chem Soc. 2010;132(37):13008-15. DOI: 10.1021/ja105340b
146. Valdés Á, Qu ZW, Kroes GJ, Rossmeisl J, Nørskov JK. Oxidation and Photo-Oxidation of Water on TiO_2 Surface. J Phys Chem C. 2008;112(26):9872-9. DOI: 10.1021/jp711929d
147. Li Y-F, Selloni A. Pathway of Photocatalytic Oxygen Evolution on Aqueous TiO_2 Anatase and Insights into the Different Activities of Anatase and Rutile. ACS Catal. 2016;6(7):4769-74. DOI: 10.1021/acscatal.6b01138
148. Imanishi A, Okamura T, Ohashi N, Nakamura R, Nakato Y. Mechanism of Water Photooxidation Reaction at Atomically Flat TiO_2 (Rutile) (110) and (100) Surfaces: Dependence on Solution pH. J Am Chem Soc. 2007;129(37):11569-78. DOI:

10.1021/ja073206+
149. Nakamura R, Okamura T, Ohashi N, Imanishi A, Nakato Y. Molecular Mechanisms of Photoinduced Oxygen Evolution, Pl Emission, and Surface Roughening at Atomically Smooth (110) and (100) n-TiO_2 (Rutile) Surfaces in Aqueous Acidic Solutions. J Am Chem Soc. 2005;127(37):12975-83. DOI: 10.1021/ja053252e
150. Nakamura R, Nakato Y. Primary Intermediates of Oxygen Photoevolution Reaction on TiO_2 (Rutile) Particles, Revealed by in situ FTIR Absorption and Photoluminescence Measurements. J Am Chem Soc. 2004;126(4):1290-8. DOI: 10.1021/ja0388764
151. Stecher T, Reuter K, Oberhofer H. First-Principles Free-Energy Barriers for Photoelectrochemical Surface Reactions: Proton Abstraction at TiO_2 (110). Phys Rev Lett. 2016;117(27):276001. DOI: 10.1103/PhysRevLett.117.276001
152. Wang H-L, Hu Z-P, Li H. Dissociation of Liquid Water on Defective Rutile TiO_2 (110) Surfaces Using Ab Initio Molecular Dynamics Simulations. Front Phys. 2018;13(3):138107. DOI: 10.1007/s11467-018-0763-5
153. Selcuk S, Selloni A. Facet-Dependent Trapping and Dynamics of Excess Electrons at Anatase TiO_2 Surfaces and Aqueous Interfaces. Nat Mater. 2016;15:1107. DOI: 10.1038/nmat4672
154. Mücksch C, Urbassek HM. Accelerated Molecular Dynamics Study of the Effects of Surface Hydrophilicity on Protein Adsorption. Langmuir. 2016;32(36):9156-62. DOI: 10.1021/acs.langmuir.6b02229
155. YazdanYar A, Aschauer U, Bowen P. Adsorption Free Energy of Single Amino Acids at the Rutile (110)/Water Interface Studied by Well-Tempered Metadynamics. J Phys Chem C. 2018;122(21):11355-63. DOI: 10.1021/acs.jpcc.7b12614
156. Zheng T, Wu C, Chen M, Zhang Y, Cummings PT. Molecular Mechanics of the Cooperative Adsorption of a Pro-Hyp-Gly Tripeptide on a Hydroxylated Rutile TiO_2(110) Surface Mediated by Calcium Ions. Phys Chem Chem Phys. 2016;18(29):19757-64. DOI: 10.1039/C6CP03046G
157. Wang M, Wang Q, Wang K, Lu X. Functionalized TiO_2 Surfaces Facilitate Selective Receptor-Recognition and Modulate Biological Function of Bone

Morphogenetic Protein-2. J Phys Chem C. 2018;122(51):29319-29. DOI: 10.1021/acs.jpcc.8b09492

158. Mysen B, Richet P. Chapter 9 - Structure of Aluminosilicate Glass and Melt. Silicate Glasses and Melts (Second Edition): Elsevier; 2019. p. 301-48. DOI: https://doi.org/10.1016/B978-0-444-63708-6.00009-0

159. Quezada GR, Rozas RE, Toledo PG. Ab Initio Calculations of Partial Charges at Kaolinite Edge Sites and Molecular Dynamics Simulations of Cation Adsorption in Saline Solutions at and above the pH of Zero Charge. J Phys Chem C. 2019;123(37):22971-80. DOI: 10.1021/acs.jpcc.9b05339

160. Chen Z, Zhao Y, Xu X, Liu C, Yang L. Structure and Dynamics of Cs^+ in Kaolinite: Insights from Molecular Dynamics Simulations. Comput Mater Sci. 2020;171:109256. DOI: https://doi.org/10.1016/j.commatsci.2019.109256

161. Zeitler TR, Greathouse JA, Cygan RT, Fredrich JT, Jerauld GR. Molecular Dynamics Simulation of Resin Adsorption at Kaolinite Edge Sites: Effect of Surface Deprotonation on Interfacial Structure. J Phys Chem C. 2017;121(41):22787-96. DOI: 10.1021/acs.jpcc.7b06688

162. Kobayashi K, Liang Y, Amano K-i, Murata S, Matsuoka T, Takahashi S, et al. Molecular Dynamics Simulation of Atomic Force Microscopy at the Water–Muscovite Interface: Hydration Layer Structure and Force Analysis. Langmuir. 2016;32(15):3608-16. DOI: 10.1021/acs.langmuir.5b04277

163. Kobayashi K, Liang Y, Murata S, Matsuoka T, Takahashi S, Nishi N, et al. Ion Distribution and Hydration Structure in the Stern Layer on Muscovite Surface. Langmuir. 2017;33(15):3892-9. DOI: 10.1021/acs.langmuir.7b00436

164. Jia Z, Li X, Zhu C, Yang S, Yang G. Reversal of Cation-Specific Effects at the Interface of Mica and Aqueous Solutions. J Phys Chem C. 2018;122(10):5358-65. DOI: 10.1021/acs.jpcc.7b09956

165. Vogiatzis KD, Polynski MV, Kirkland JK, Townsend J, Hashemi A, Liu C, et al. Computational Approach to Molecular Catalysis by 3d Transition Metals: Challenges and Opportunities. Chem Rev. 2019;119(4):2453-523. DOI: 10.1021/acs.chemrev.8b00361

166. Szabová L, Tateyama Y, Matolín V, Fabris S. Water Adsorption and Dissociation

at Metal-Supported Ceria Thin Films: Thickness and Interface-Proximity Effects Studied with DFT+U Calculations. J Phys Chem C. 2015;119(5):2537-44. DOI: 10.1021/jp5109152

167. Farnesi Camellone M, Negreiros Ribeiro F, Szabová L, Tateyama Y, Fabris S. Catalytic Proton Dynamics at the Water/Solid Interface of Ceria-Supported Pt Clusters. J Am Chem Soc. 2016;138(36):11560-7. DOI: 10.1021/jacs.6b03446

168. Szabová L, Camellone MF, Ribeiro FN, Matolín V, Tateyama Y, Fabris S. Dynamical Solvent Effects on the Charge and Reactivity of Ceria-Supported Pt Nanoclusters. J Phys Chem C. 2018;122(48):27507-15. DOI: 10.1021/acs.jpcc.8b09154

169. Muñoz-Santiburcio D, Farnesi Camellone M, Marx D. Solvation-Induced Changes in the Mechanism of Alcohol Oxidation at Gold/Titania Nanocatalysts in the Aqueous Phase Versus Gas Phase. Angew Chem Int Ed. 2018;57(13):3327-31. DOI: 10.1002/anie.201710791

170. Cai Q, Lopez-Ruiz JA, Cooper AR, Wang J-g, Albrecht KO, Mei D. Aqueous-Phase Acetic Acid Ketonization over Monoclinic Zirconia. ACS Catal. 2017;8(1):488-502. DOI: 10.1021/acscatal.7b03298

171. Kitadai N, Oonishi H, Umemoto K, Usui T, Fukushi K, Nakashima S. Glycine Polymerization on Oxide Minerals. Origins of Life and Evolution of Biospheres. 2017;47(2):123-43. DOI: 10.1007/s11084-016-9516-z

172. Erastova V, Degiacomi MT, Fraser D, Greenwell HC. Mineral Surface Chemistry Control for Origin of Prebiotic Peptides. Nat Commun. 2017;8(1):2033. DOI: 10.1038/s41467-017-02248-y

173. Wang H, Ma C, Zhou L. A Brief Review of Machine Learning and Its Application. 2009 International Conference on Information Engineering and Computer Science; 2009 19-20 Dec. 2009. DOI: 10.1109/ICIECS.2009.5362936

174. Behler J, Parrinello M. Generalized Neural-Network Representation of High-Dimensional Potential-Energy Surfaces. Phys Rev Lett. 2007;98(14):146401. DOI: 10.1103/PhysRevLett.98.146401

175. Behler J. Constructing High-Dimensional Neural Network Potentials: A Tutorial Review. Int J Quantum Chem. 2015;115(16):1032-50. DOI: 10.1002/qua.24890

176. Jiequn H, Linfeng Z, Roberto C, Weinan E. Deep Potential: A General Representation of a Many-Body Potential Energy Surface. Commun Comput Phys. 2018;23(3):629--39. DOI: https://doi.org/10.4208/cicp.OA-2017-0213

177. Zhang L, Han J, Wang H, Car R, E W. Deep Potential Molecular Dynamics: A Scalable Model with the Accuracy of Quantum Mechanics. Phys Rev Lett. 2018;120(14):143001. DOI: 10.1103/PhysRevLett.120.143001

178. Lu D, Wang H, Chen M, Lin L, Car R, E W, et al. 86 PFLOPS Deep Potential Molecular Dynamics Simulation of 100 Million Atoms with Ab Initio Accuracy. Comput Phys Commun. 2021;259:107624. DOI: https://doi.org/10.1016/j.cpc.2020.107624

179. Quaranta V, Hellström M, Behler J. Proton-Transfer Mechanisms at the Water–ZnO Interface: The Role of Presolvation. J Phys Chem Lett. 2017;8(7):1476-83. DOI: 10.1021/acs.jpclett.7b00358

180. Hellström M, Quaranta V, Behler J. One-Dimensional vs. Two-Dimensional Proton Transport Processes at Solid–Liquid Zinc-Oxide–Water Interfaces. Chem Sci. 2019;10(4):1232-43. DOI: 10.1039/C8SC03033B

181. Quaranta V, Behler J, Hellström M. Structure and Dynamics of the Liquid–Water/Zinc-Oxide Interface from Machine Learning Potential Simulations. J Phys Chem C. 2019;123(2):1293-304. DOI: 10.1021/acs.jpcc.8b10781

182. Singraber A, Behler J, Dellago C. Library-Based LAMMPS Implementation of High-Dimensional Neural Network Potentials. J Chem Theory Comput. 2019;15(3):1827-40. DOI: 10.1021/acs.jctc.8b00770

183. Qi Y, Lee J, Klauda JB, Im W. CHARMM-GUI Nanodisc Builder for Modeling and Simulation of Various Nanodisc Systems. J Comput Chem. 2019;40(7):893-9. DOI: https://doi.org/10.1002/jcc.25773

184. O'Connor M, Deeks HM, Dawn E, Metatla O, Roudaut A, Sutton M, et al. Sampling Molecular Conformations and Dynamics in a Multiuser Virtual Reality Framework. Science Advances. 2018;4(6):eaat2731. DOI: 10.1126/sciadv.aat2731